

# Energy Model-based Accurate Shapley Value Estimation for Interpretable Deep Learning Predictive Modelling

Cheng Lu, Jiusun Zeng, Yu Xia, Jinhui Cai, Shihua Luo

**Abstract**—As a favorable tool for explainable artificial intelligence (XAI), Shapley value has been widely used to interpret deep learning based predictive models. However, accurate and efficient estimation of Shapley value is a difficult task since the computation load grows exponentially with the increase of input features. Most existing accelerated Shapley value estimation methods have to compromise on estimation accuracy with efficiency. In this article, we present EmSHAP(Energy model-based Shapley value estimation), which can effectively approximate the expectation of Shapley contribution function/deep learning model under arbitrary subset of features given the rest. In order to determine the proposal conditional distribution in the energy model, a gated recurrent unit(GRU) is introduced by mapping the input features onto a hidden space, so that the impact of input feature orderings can be eliminated. In addition, a dynamic masking scheme is proposed to improve the generalization ability. It is proved in Theorems 1, 2 and 3 that EmSHAP achieves tighter error bound than state-of-the-art methods like KernelSHAP and VAEAC, leading to higher estimation accuracy. Finally, case studies on a medical application and an industrial application show that the proposed Shapley value-based explainable framework exhibits enhanced estimation accuracy without compromise on efficiency.

**Index Terms**—Explainable artificial intelligence, deep learning, Shapley value, energy model.

## I. INTRODUCTION

Deep learning has been extensively applied in many complex supervised learning problems like medical diagnosis [1], industrial intelligence [2], financial modeling [3] etc. Deep learning models outperform conventional methods in terms of predictive accuracy in many cases, however, since most deep learning models are black box and have complicated structure, interpretation of the predictive results becomes difficult. This limitation poses challenges in identifying key features that influence the predictive model and understanding the relationship between input features and output predictions. The interpretability requirements lead to the development of an active research area of Explainable Artificial Intelligence (XAI) [4].

In XAI, the concept of model interpretability lacks a clear mathematical formulation. Nevertheless, there is a general consensus on the formulation proposed by Doshi-Velez *et al.* [5].

This work was supported in part by xxx (xxx). (*Corresponding author: Jiusun Zeng*)

Cheng Lu and Jinhui Cai are with the College of Metrology and Measurement Engineering, China Jiliang University, Hangzhou, 310018, China. (lucheng.cjlu@gmail.com, caijinhui@cjlu.edu.cn)

Jiusun Zeng, Yu Xia are with the School of Mathematics, Hangzhou Normal University, Hangzhou, 311121, China. (jszeng@hznu.edu.cn, xia@hznu.edu.cn)

Shihua Luo is with the School of Statistics, Jiangxi University of Finance and Economics, Nanchang, 330013, China. (luoshihua@aliyun.com)

According to Doshi-Velez *et al.* [5], an explanation algorithm is considered trustworthy if it accurately reveals the underlying reasoning behind a model’s decisions. In this regard, the Shapley value-based explanation becomes popular due to its rigid mathematical foundation and theoretical basis. Originated from the field of cooperative games [6] and reintroduced as an explanation framework [7], the Shapley value effectively overcomes the limitations of black-box models through the implementation of fair allocation schemes. Although the utilization of Shapley values for explaining deep learning models may lead to non-intuitive feature attributions [8]–[10], the ideal mathematical properties of Shapley make it possible to fairly measure the contribution of each input in the model using this method. Consequently, interpretable approaches based on Shapley value remain a popular method.

A notable problem for Shapley-based explanation is its high computation load. By definition, the computational complexity of Shapley value increases exponentially with the number of variables. In order to accelerate computation, a series of statistical based methods have been developed that can be roughly divided into three categories: regression-based methods, sampling-based methods, and structure model-based methods. Regression-based methods employ weighted linear regression to accelerate the estimation of Shapley value, with examples including SHAP (SHapley Additive exPlanation) [11] and KernelSHAP [12]. Sampling-based methods utilize Monte Carlo sampling to approximate the true Shapley value. These methods involve Monte Carlo approximation using randomly sampled permutations [13] or sampling based on random permutations of local features [14]. On the other hand, structure model-based methods leverage specific model structure constraints to approximate the Shapley value. Examples of such methods include tree Shapley [15] and graph Shapley [16]. More recently, a generative model for Shapley value estimation based on variational autoencoder with arbitrary conditioning (VAEAC) [17] has been developed, which uses a single model for all feature combinations and consequently reduces computation burden. A comprehensive literature review on Shapley-based explanation methods can be found in Ref. [18].

Despite the advancements made in calculation of Shapley value, several significant issues still remain. For example, regression-based methods can improve the estimation efficiency of Shapley value, however, the inherent assumption of independence among variables may negatively affect its accuracy. Sampling-based methods require large quantity of samplings to achieve sufficient accuracy, and hence have high computation load. Whilst structure model-based approaches demonstrate improved efficiency, their application scenarios

are limited to specific models. For VAEAC, it can reduce computation burden, but suffers from two issues: i) The distribution of hidden space in variational autoencoder (VAE) is unimodal Gaussian, and cannot handle data with complex distributions; ii) An autoregressive model is applied for estimating the conditional distribution of each feature given the rest, whose estimation accuracy heavily relies on the structure of the autoregressive model. Another notable issue is that there still lacks rigid theoretical analysis on the error bounds of different Shapley value-based approaches, making it difficult to evaluate their accuracies.

In order to better tradeoff between computation efficiency and estimation accuracy, this article presents the EmSHAP(Energy model-based SHapley value estimation), which falls into the class of generative model based approach [17]. The method relies on the energy model to obtain the expectation of Shapley contribution function/conditional Shapley value under some arbitrary subset of features given the rest. In order to reduce the impact of feature orderings to the estimation of proposal conditional distribution in the energy model, a GRU is introduced by mapping the input features onto a hidden space. A dynamic masking scheme is further introduced to improve the generalization ability. The advantages and merits can be summarized as follows: i) The energy model can handle arbitrary data distributions; ii) The introduction of GRU can avoid the impact of feature ordering, leading to more accurate estimation; iii) The dynamic masking scheme can improve the model generalization performance by a progressive adjustment of the masking ratio based on the training epoch. More importantly, to provide an evaluation criterion for estimation accuracies of different methods, theoretical analysis on error bounds of EmSHAP, KernelSHAP and VAEAC are performed and shown in Theorems 1, 2 and 3. The tighter error bound of EmSHAP indicates that it is more accurate than competitive methods. The performance of the proposed method is further verified in application studies to a medical example and an industrial example, which confirmed its higher estimation accuracy as well as good efficiency.

## II. PRELIMINARIES

In this section, preliminary knowledge about Shapley value based explanation framework, energy-based model and GRU is provided.

### A. Shapley value

Shapley value is a tool from game theory designed to fairly allocate the contribution generated by a coalition game among its individual players [6]. Suppose a total of  $d$  players participate in the game, and these players form a set of  $D = \{1, \dots, d\}$ , the contribution of these players in this game can be quantified as  $v(D)$  and the revenue of the player subset  $S (S \subseteq D)$  is  $v(S)$ , with  $v(\cdot)$  being a predefined contribution function. The Shapley value is defined as the player' marginal contribution to the payoff of all possible player subsets. The definition of the Shapley value is as follows.

$$\phi_i = \sum_{S \subseteq D \setminus \{i\}} \frac{|S|!(|D| - |S| - 1)!}{|D|!} (v(S \cup \{i\}) - v(S)) \quad (1)$$

Here,  $\phi_i$  is the Shapley value of the  $i$ -th player,  $|S|$  is the number of players in subset  $S$ , and  $|D|$  is the number of all players. The definition of Eq.(1) renders Shapley value the following favorable properties.

- **Efficiency:** The sum of Shapley values for players from a subset is equal to the difference between the contribution function of the collection of these players and the contribution function of the empty set, i.e.  $\sum_{i=1}^{|S|} \phi_i = v(S) - v(\emptyset)$ ;
- **Symmetry:** For any coalition  $S$  not containing  $i_1$  and  $i_2$ , if player  $i_1$  and player  $i_2$  satisfy  $v(S \cup \{i_1\}) = v(S \cup \{i_2\})$ , then  $\phi_{i_1} = \phi_{i_2}$ ;
- **Dummy:** Regardless of which coalition of players it is added to, a player  $i$  does not change the contribution value, that is  $v(S) = v(S \cup \{i\})$  for any coalition  $S$ , then  $\phi_i = 0$ ;
- **Additivity:** For a game with combined contribution function  $v_1 + v_2$ , the Shapley value can be calculated by  $\phi_{i_1} + \phi_{i_2}$ .

### B. Shapley value-based model explanation

Let  $\tilde{f} : \mathbf{x} \in \mathbb{R}^{|D|} \rightarrow y \in \mathbb{R}$  be an unknown data generating function that generates a set of  $n$  measurements of input features  $\mathbf{X} = \{\mathbf{x}_t\}_{t=1}^n, \mathbf{x}_t \in \mathbb{R}^{|D|}$  and output feature  $\mathbf{Y} = \{y_t\}_{t=1}^n, y_t \in \mathbb{R}$ , and  $y_t = \tilde{f}(\mathbf{x}_t)$ .  $D$  is the input feature set and  $|D|$  is the number of features. In a predictive task, the purpose is to approximate the unknown function  $\tilde{f}$  using a specific model  $\hat{y} = f(\mathbf{x})$  to minimize the approximation error between  $y$  and  $\hat{y}$  as well as the out-of-sample generalization error. The approximation/predictive model  $f(\cdot)$  can be of any type of machine learning models, in this paper, deep learning models are specifically considered.

In Shapley value-based model explanation framework, the  $|D|$  input features are related to the  $|D|$  players, the predictive model  $f(\cdot)$  is the cooperative game and the model output  $\hat{y}$  can be regarded as the sum of contribution(or Shapley values) from all features in  $\mathbf{x}$ . Noting that the framework is model-agnostic, it can be used to interpret a range of deep learning models including convolution neural networks (CNN), autoencoders(AE), long short term memory networks(LSTM), etc.

By decomposing the model output into the sum of Shapley value associated with each input feature, the output for a specific sample point  $\mathbf{x}^*$  can be expressed as follows.

$$f(\mathbf{x}^*) = \phi_0 + \sum_{i=1}^{|D|} \phi_i^* \quad (2)$$

Here,  $\phi_0$  is the base value of the model predictions and can be regarded as the expectation of global prediction [11], with  $\phi_0 = \mathbb{E}[f(\mathbf{x})]$ ,  $\phi_i^*$  is the Shapley value of the  $i$ th input feature  $x_i^*$ . Eq.(2) highlights the disparity between the model output and the global prediction by employing the Shapley value associated with each feature in  $\mathbf{x}^*$ .

To calculate  $\phi_i^*$ , an appropriate contribution function  $v(S)$  should be determined. Since  $f(\mathbf{x}^*)$  is the sum of contribution from all input features, we can easily relate  $v(\cdot)$  to  $f(\cdot)$ , that is,  $v(D) = f(\mathbf{x}^*)$  for a specific sample and  $\bar{v}(D) = \mathbb{E}[f(\mathbf{x})]$  for global prediction. Following Lundberg and Lee [11], the

contribution function can be reformed as the expected outcome of  $f(\mathbf{x})$  conditioned on the variables in  $S$  taking on specific values  $\mathbf{x}_S^*$  as follows.

$$\begin{aligned} v(S) &= \mathbb{E}[f(\mathbf{x})|\mathbf{x}_S = \mathbf{x}_S^*] = \mathbb{E}[f(\mathbf{x}_{\bar{S}}, \mathbf{x}_S)|\mathbf{x}_S = \mathbf{x}_S^*] \\ &= \int f(\mathbf{x}_{\bar{S}}, \mathbf{x}_S^*) p(\mathbf{x}_{\bar{S}}|\mathbf{x}_S = \mathbf{x}_S^*) d\mathbf{x}_{\bar{S}} \end{aligned} \quad (3)$$

where  $p(\mathbf{x}_{\bar{S}}|\mathbf{x}_S = \mathbf{x}_S^*)$  is the conditional density of  $\mathbf{x}_{\bar{S}}$  given  $\mathbf{x}_S^*$ ,  $\mathbf{x}_S$  and  $\mathbf{x}_S^*$  contains the part of inputs  $\mathbf{x}$  and  $\mathbf{x}^*$  corresponding to features inside  $S$ ,  $\mathbf{x}_{\bar{S}}$  and  $\mathbf{x}_S^*$  relate to the part of inputs in  $\mathbf{x}$  and  $\mathbf{x}^*$  corresponding to features outside  $S$ ,  $S \cup \bar{S} = D$  and  $S \cap \bar{S} = \emptyset$ .

The Shapley value provides a fair assessment of each variable's contribution to the predictive model. However, from Eq. (1) it can be seen that its estimation involves high computation load as there are a total of  $2^{|D|-1}$  combinations of  $S$ . The computational complexity will increase exponentially as the number of input features grow.

### C. Energy-based model

An energy-based model is a concept originated from statistical physics [19]. It provides a convenient tool to learn an underlying distribution from data samples. Assume the  $n$  measurements of input features are sampled from an unknown data distribution, i.e.,  $\mathbf{x} \sim p_{data}(\mathbf{x})$ , the goal of energy-based model is to learn an unnormalized density  $e^{-g_{\theta}(\mathbf{x})}$  as a parametric approximation to  $p_{data}(\mathbf{x})$ .

$$p_{data}(\mathbf{x}) \approx p_{\theta}(\mathbf{x}) = \frac{e^{-g_{\theta}(\mathbf{x})}}{Z} \quad (4)$$

where  $\theta$  are the model parameters,  $Z = \int e^{-g_{\theta}(\mathbf{x})} d\mathbf{x}$  is the partition function,  $p_{\theta}(\mathbf{x})$  is the approximated distribution, and  $g_{\theta}(\mathbf{x})$  is the energy function, which can be described by different network architecture such as multi-layer perceptron (MLP) [20]. Boltzmann machines [21] and Markov random fields [22] are typical examples of energy-based models.

The parameters in an energy-based model in Eq.(4) can be estimated by maximum likelihood estimation (MLE). Specifically, if  $\mathbf{x}_t \sim p_{data}(\mathbf{x})$  for  $t = 1, 2, \dots, n$ , the likelihood function can be expressed as,

$$\mathcal{L}(\theta) = \frac{1}{n} \sum_{t=1}^n \log p_{\theta}(\mathbf{x}_t) = \mathbb{E}_{\mathbf{x} \sim p_{data}} [\log p_{\theta}(\mathbf{x})] \quad (5)$$

Since the energy function  $g_{\theta}(\mathbf{x})$  in Eq.(4) can use different network architecture, it can approximate any kind of data distribution. In addition, the energy function can be multimodal without resorting to mixture distributions and does not differentiate between discrete and continuous distributions. These advantages make the energy-based model more flexible than the traditional distribution approximation methods.

### D. Gated recurrent unit (GRU)

GRU network [23] is a typical modification of the recurrent neural network (RNN), which uses the update and reset gates to adaptively update its hidden state, allowing it to capture and propagate relevant information through sequential data. More precisely, the update gate controls adjustments to the hidden

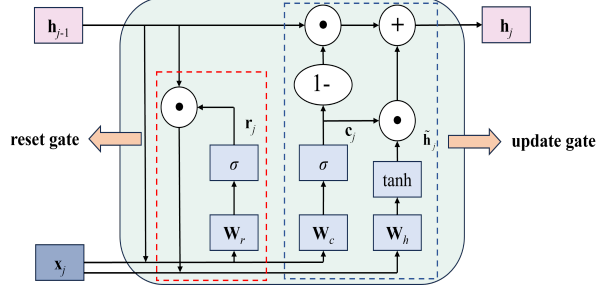


Fig. 1. Structure of GRU cell

layer state, while the reset gate decides whether to disregard the previous hidden layer state. A general structure of GRU cell is shown in Fig. 1 and the parameters updating equations are specified as follows.

$$\begin{aligned} \mathbf{r}_j &= \sigma(\mathbf{W}_r \cdot [\mathbf{h}_{j-1}, \mathbf{x}_j] + \mathbf{b}_r) \\ \mathbf{c}_j &= \sigma(\mathbf{W}_c \cdot [\mathbf{h}_{j-1}, \mathbf{x}_j] + \mathbf{b}_c) \\ \tilde{\mathbf{h}}_j &= \tanh(\mathbf{W}_h \cdot [\mathbf{r}_j \cdot \mathbf{h}_{j-1}, \mathbf{x}_j] + \mathbf{b}_h) \\ \mathbf{h}_j &= (1 - \mathbf{c}_j) \cdot \mathbf{h}_{j-1} + \mathbf{c}_j \cdot \tilde{\mathbf{h}}_j \end{aligned} \quad (6)$$

where,  $\mathbf{c}_j$  and  $\mathbf{r}_j$  are the update gate and reset gate, respectively,  $j$  is the index of GRU cell.  $\mathbf{h}_j$  is the current hidden layer,  $\mathbf{h}_{j-1}$  is the previous hidden layer.  $\mathbf{x}_j$  is the current input.  $\mathbf{W}_r$ ,  $\mathbf{W}_c$ , and  $\mathbf{W}_h$  are the weight parameters in GRU.  $\sigma$  is the sigmoid activation function,  $\tanh$  is the tanh activate function.  $\mathbf{b}_r$ ,  $\mathbf{b}_c$ , and  $\mathbf{b}_h$  are the bias term in GRU.  $\mathbf{W}$  and  $\mathbf{b}$  are determined in the training process.

### III. ESTIMATE SHAPLEY VALUE USING EMSHAP

By definition of Shapley value in Eq.(1), it can be seen that the most important step is to estimate the contribution function  $v(S)$ , which can be reformulated as the conditional expectation in Eq.(3). The conditional expectation can be empirically approximated by techniques like Monte Carlo integration provided the conditional probability  $p(\mathbf{x}_{\bar{S}}|\mathbf{x}_S^*)$  is known.

$$\begin{aligned} v(S) &= \mathbb{E}[f(\mathbf{x}_{\bar{S}}, \mathbf{x}_S)|\mathbf{x}_S = \mathbf{x}_S^*] = \int f(\mathbf{x}_{\bar{S}}, \mathbf{x}_S^*) p(\mathbf{x}_{\bar{S}}|\mathbf{x}_S = \mathbf{x}_S^*) d\mathbf{x}_{\bar{S}} \\ &\approx \hat{v}(S) = \frac{1}{K} \sum_{k=1}^K f(\mathbf{x}_{\bar{S}}^{(k)}, \mathbf{x}_S^*) \end{aligned} \quad (7)$$

where  $\mathbf{x}_{\bar{S}}^{(k)} \sim p(\mathbf{x}_{\bar{S}}|\mathbf{x}_S = \mathbf{x}_S^*)$  for  $k = 1, 2, \dots, K$ , and  $K$  is the number of Monte Carlo sampling. It is worth noting that estimation of conditional density  $p(\mathbf{x}_{\bar{S}}|\mathbf{x}_S)$  can be achieved by using kernel density estimation (KDE) [24]. However, KDE is computationally challenging for high dimensional inputs. More importantly, using KDE requires estimation of  $2^{|D|} - 2$  conditional densities as there are a total of  $2^{|D|} - 2$  combinations of  $S$ . Instead, an energy-based model called EmSHAP is presented here, which is capable of estimating all conditional densities using a single model. It has the network structure as shown in Fig. 2.

In Fig. 2, data batches of input features is fed into the energy network to estimate the energy function  $\exp(-g_{\theta}(\mathbf{x}_{\bar{S}}, \mathbf{x}_S))$ , which can be used to approximate the conditional probability

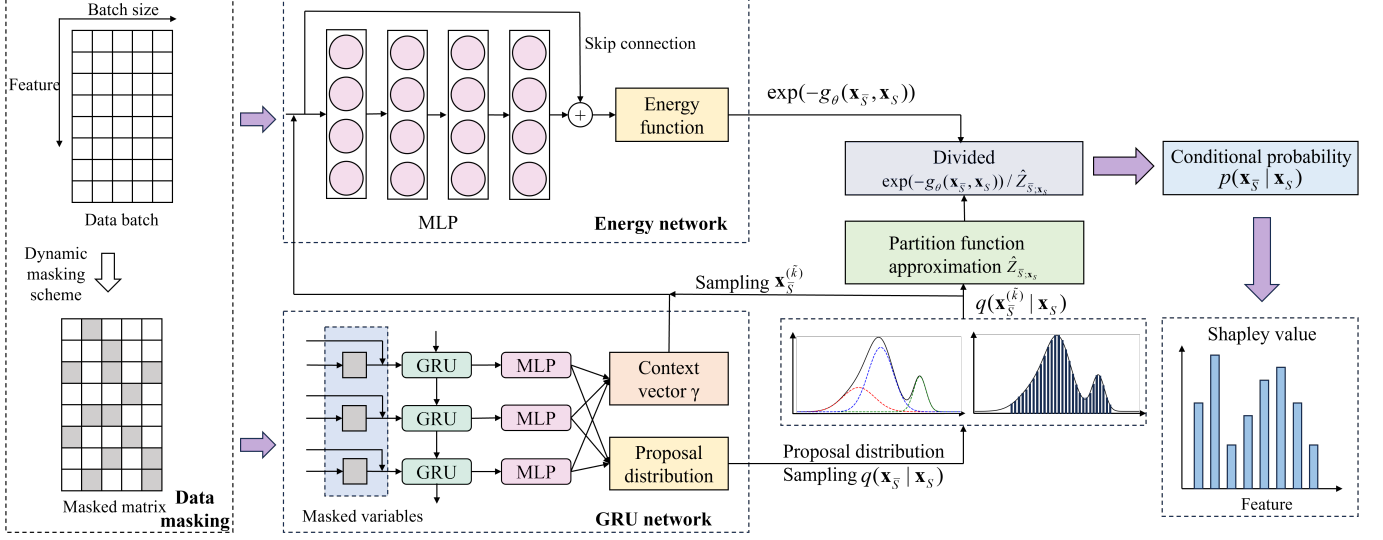


Fig. 2. Structure of GRU coupled energy-based model for estimating Shapley value

$p(\mathbf{x}_{\bar{S}}|\mathbf{x}_S)$  after divided by the partition function. The partition function, on the other hand, needs to be approximated by Monte Carlo integration from the proposal distribution  $q(\mathbf{x}_{\bar{S}}|\mathbf{x}_S)$ . The proposal distribution can be estimated using an autoregressive approach [25], however, its estimation accuracy will be negatively affected by the variable ordering. Instead, a GRU network with a dynamic masking scheme is used to estimate the proposal distribution, which outputs parameters related to the estimated proposal distribution and a context vector  $\gamma$ , which is used to connect the energy network and the GRU network. With the conditional probability  $p(\mathbf{x}_{\bar{S}}|\mathbf{x}_S)$  obtained, the contribution function can be estimated from Eq.(7), and Shapley value can be subsequently obtained from Eq.(1). The details of the network structure will be explained in Subsection III-A.

#### A. GRU coupled energy-based model

When using the energy model to approximate the conditional density  $p(\mathbf{x}_{\bar{S}}|\mathbf{x}_S)$ , we are interested in estimating the conditional density of inputs in  $\bar{S}$  conditioned on the remaining observed inputs (in  $S$ ), for all possible  $\bar{S}$ . According to Eq.(4),  $p(\mathbf{x}_{\bar{S}}|\mathbf{x}_S)$  can be approximated using the energy-based model as follows.

$$p(\mathbf{x}_{\bar{S}}|\mathbf{x}_S) \approx \frac{\exp(-g_{\theta}(\mathbf{x}_{\bar{S}}, \mathbf{x}_S))}{Z_{\bar{S}, \mathbf{x}_S}} \quad (8)$$

Here, the energy function  $g_{\theta}$  can be designed as an unnormalized MLP with skip connections [26], as is shown in Fig. 2. The right hand side of Eq.(8) can be transformed to a probability once  $Z_{\bar{S}, \mathbf{x}_S}$  is known, however, it is always intractable to directly calculate  $Z_{\bar{S}, \mathbf{x}_S}$ . One solution is to introduce a proposal conditional distribution  $q(\mathbf{x}_{\bar{S}}|\mathbf{x}_S)$  that is close to  $Z_{\bar{S}, \mathbf{x}_S}$ , then use Monte Carlo integration to sample from

$q(\mathbf{x}_{\bar{S}}|\mathbf{x}_S)$  to approximate  $Z_{\bar{S}, \mathbf{x}_S}$ .

$$\begin{aligned} \hat{Z}_{\bar{S}, \mathbf{x}_S} &= \int \exp(-g_{\theta}(\mathbf{x}_{\bar{S}}, \mathbf{x}_S)) d\mathbf{x}_{\bar{S}} \\ &= \int \frac{\exp(-g_{\theta}(\mathbf{x}_{\bar{S}}, \mathbf{x}_S))}{q(\mathbf{x}_{\bar{S}}|\mathbf{x}_S)} q(\mathbf{x}_{\bar{S}}|\mathbf{x}_S) d\mathbf{x}_{\bar{S}} \\ &\approx \frac{1}{\tilde{K}} \sum_{k=1}^{\tilde{K}} \frac{\exp(-g_{\theta}(\mathbf{x}_{\bar{S}}^{(k)}, \mathbf{x}_S))}{q(\mathbf{x}_{\bar{S}}^{(k)}|\mathbf{x}_S)}, \mathbf{x}_{\bar{S}}^{(k)} \sim q(\mathbf{x}_{\bar{S}}|\mathbf{x}_S) \end{aligned} \quad (9)$$

Here,  $\hat{Z}_{\bar{S}, \mathbf{x}_S}$  is the approximate partition function,  $\tilde{K}$  is the number of Monte-Carlo sampling. When  $q(\mathbf{x}_{\bar{S}}|\mathbf{x}_S)$  and  $p(\mathbf{x}_{\bar{S}}|\mathbf{x}_S)$  are close, such a sampling estimation can be regarded as unbiased. Otherwise, the sampling estimates will have a large variance. Thus, an appropriate proposal distribution  $q(\mathbf{x}_{\bar{S}}|\mathbf{x}_S)$  should be defined, which is desired to be close to  $p(\mathbf{x}_{\bar{S}}|\mathbf{x}_S)$  as much as possible and have a parametric expression that is easy to be inferred.

The proposal distribution  $q(\mathbf{x}_{\bar{S}}|\mathbf{x}_S)$  can be obtained through an autoregressive approach [25],

$$q(\mathbf{x}_{\bar{S}}|\mathbf{x}_S) \approx \prod_{j=1}^{|\bar{S}|} q(\mathbf{x}_{\bar{S}_j}|\mathbf{x}_{S \cup \bar{S}_{<j}}) \quad (10)$$

Eq.(10) uses the chain rule of conditional probability to obtain the proposal distribution, so that estimation of the proposal distribution can be converted into the multiplication of a series of one-dimensional probabilities  $q(\mathbf{x}_{\bar{S}_j}|\mathbf{x}_{S \cup \bar{S}_{<j}})$ , which is easy and tractable.

An important issue arises here, namely, the variable ordering of the conditional probabilities  $q(\mathbf{x}_{\bar{S}_j}|\mathbf{x}_{S \cup \bar{S}_{<j}})$  will have a significant impact on the estimation results. For example, for a predictive task with three inputs  $x_1$ ,  $x_2$  and  $x_3$ , when calculating the conditional density  $q(x_2, x_3|x_1)$ , it can be obtained as  $q(x_2, x_3|x_1) = q(x_3|x_1, x_2)q(x_2|x_1)$  or  $q(x_2, x_3|x_1) = q(x_2|x_1, x_3)q(x_3|x_1)$  according to different variable orderings. Theoretically,  $q(x_3|x_1, x_2)q(x_2|x_1)$  is equal to  $q(x_2|x_1, x_3)q(x_3|x_1)$ , however, since we use the energy-based model to approximate the distributions, the two orderings may

produce different results. This is problematic if the number of input features is large. Though Ryan *et al.* [25] used plenty of random training to alleviate this problem, the solution is still unsatisfactory.

In order to better estimate the conditional distribution and subsequently the Shapley value, a GRU network with a masking scheme is applied here. Fig. 3 displays the GRU network to approximate  $q(\mathbf{x}_{\bar{S}}|\mathbf{x}_S)$  for a set of 8 variables, where  $\bar{S} = \{\mathbf{x}_2, \mathbf{x}_5, \mathbf{x}_8\}$  are called the masked variables and  $S = \{\mathbf{x}_1, \mathbf{x}_3, \mathbf{x}_4, \mathbf{x}_6, \mathbf{x}_7\}$  are the unmasked variables.

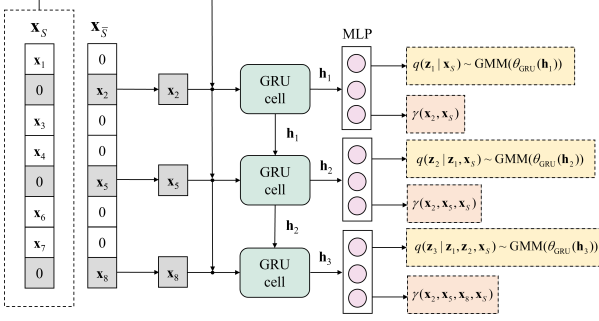


Fig. 3. GRU network for proposal distribution estimation

The GRU network models the diverse dependencies among variables through a series of GRU cells. This enables estimation of conditional probability between a masked variable and the unmasked variables to be conceptualized as a simple loop. It maps the variables into a latent space and utilizes the chain rule within the latent space to eliminate the impact of input feature orderings.

In Fig. 3, together with the unmasked variables, each masked variable is fed into a separate GRU cell to obtain a hidden state  $\mathbf{h}$ . Specifically, The input and output of  $j$ -GRU cell are as follows.

$$\mathbf{h}_j = \text{GRU}(\mathbf{x}_{\bar{S}_j}, \mathbf{x}_{S \cup \bar{S}_{<j}}, \mathbf{h}_{j-1}) \quad (11)$$

where  $\mathbf{h}_j$  is the output of the  $j$ -th GRU cell. The hidden state  $\mathbf{h}$  goes through a fully connected MLP and outputs the weight, mean and variance parameters of the Gaussian mixture model (GMM) to get a conditional density  $q(\mathbf{z}|\mathbf{x}_S)$  and a context vector  $\gamma$ . The conditional density is obtained as follows.

$$q(\mathbf{z}_{\bar{S}_j} | \mathbf{z}_{\bar{S}_{j-1}}, \dots, \mathbf{z}_{\bar{S}_1}, \mathbf{x}_S) = \text{GMM}(\mathbf{z}_{\bar{S}_j} | \text{MLP}(\mathbf{h}_j)) \quad (12)$$

And the proposal distribution can be obtained using the following chain rule.

$$q(\mathbf{x}_{\bar{S}} | \mathbf{x}_S) = \prod_{j=1}^{|\bar{S}|} q(\mathbf{z}_{\bar{S}_j} | \mathbf{z}_{\bar{S}_{j-1}}, \dots, \mathbf{z}_{\bar{S}_1}, \mathbf{x}_S) \quad (13)$$

With the proposal distribution  $q(\mathbf{x}_{\bar{S}} | \mathbf{x}_S)$  determined, the loss function of the GRU network can be established according to the maximum likelihood criterior.

$$\begin{aligned} \mathcal{J}(\Theta; \mathbf{x}) &= -\mathcal{L}(\Theta; \mathbf{x}) = \\ &= -\frac{1}{K} \sum_{j \in \bar{S}} \sum_{k=1}^K \log p(\mathbf{x}_{\bar{S}_j}^{(k)} | \mathbf{x}_S, \Theta) - \sum_{j \in \bar{S}} \log q(\mathbf{x}_{\bar{S}_j} | \mathbf{x}_S, \Theta) \end{aligned} \quad (14)$$

Here  $\Theta$  is the parameter set.

Using the GRU network structure in Fig. 3, the conditional densities for any combination of  $\mathbf{x}_{\bar{S}}$  given  $\mathbf{x}_S$  can be obtained by discarding the GRU cells corresponding to unrelated masked variables in  $\mathbf{x}_{\bar{S}}$ , so that a single model can estimate all the conditional densities and repetitive operation of conditional density estimations can be avoided.

In addition, the difference in the variance of the data sampled from the proposal conditional distribution and the true conditional distribution has an explicit expression. Specifically, The data sampled from the true conditional distribution has the following variance,

$$\begin{aligned} &Var_{\mathbf{x}_{\bar{S}} \sim p(\mathbf{x}_{\bar{S}} | \mathbf{x}_S)} [Z_{\bar{S}; \mathbf{x}_S}] \\ &= \mathbb{E}_{\mathbf{x}_{\bar{S}} \sim p(\mathbf{x}_{\bar{S}} | \mathbf{x}_S)} [Z_{\bar{S}; \mathbf{x}_S}^2] - \left( \mathbb{E}_{\mathbf{x}_{\bar{S}} \sim p(\mathbf{x}_{\bar{S}} | \mathbf{x}_S)} [Z_{\bar{S}; \mathbf{x}_S}] \right)^2 \end{aligned} \quad (15)$$

Meanwhile, the variance of the data sampled from the proposal conditional distribution is,

$$\begin{aligned} &Var_{\mathbf{x}_{\bar{S}} \sim q(\mathbf{x}_{\bar{S}} | \mathbf{x}_S)} \left[ Z_{\bar{S}; \mathbf{x}_S} \frac{p(\mathbf{x}_{\bar{S}} | \mathbf{x}_S)}{q(\mathbf{x}_{\bar{S}} | \mathbf{x}_S)} \right] \\ &= \mathbb{E}_{\mathbf{x}_{\bar{S}} \sim q(\mathbf{x}_{\bar{S}} | \mathbf{x}_S)} \left[ \left( Z_{\bar{S}; \mathbf{x}_S} \frac{p(\mathbf{x}_{\bar{S}} | \mathbf{x}_S)}{q(\mathbf{x}_{\bar{S}} | \mathbf{x}_S)} \right)^2 \right] \\ &\quad - \left( \mathbb{E}_{\mathbf{x}_{\bar{S}} \sim q(\mathbf{x}_{\bar{S}} | \mathbf{x}_S)} \left[ Z_{\bar{S}; \mathbf{x}_S} \frac{p(\mathbf{x}_{\bar{S}} | \mathbf{x}_S)}{q(\mathbf{x}_{\bar{S}} | \mathbf{x}_S)} \right] \right)^2 \\ &= \mathbb{E}_{\mathbf{x}_{\bar{S}} \sim p(\mathbf{x}_{\bar{S}} | \mathbf{x}_S)} \left[ Z_{\bar{S}; \mathbf{x}_S}^2 \frac{p(\mathbf{x}_{\bar{S}} | \mathbf{x}_S)}{q(\mathbf{x}_{\bar{S}} | \mathbf{x}_S)} \right] \\ &\quad - \left( \mathbb{E}_{\mathbf{x}_{\bar{S}} \sim p(\mathbf{x}_{\bar{S}} | \mathbf{x}_S)} [Z_{\bar{S}; \mathbf{x}_S}] \right)^2 \end{aligned} \quad (16)$$

Subtract Eq.(15) and Eq.(16), the following equation is obtained:

$$\begin{aligned} &Var_{\mathbf{x}_{\bar{S}} \sim p(\mathbf{x}_{\bar{S}} | \mathbf{x}_S)} [Z_{\bar{S}; \mathbf{x}_S}] - Var_{\mathbf{x}_{\bar{S}} \sim q(\mathbf{x}_{\bar{S}} | \mathbf{x}_S)} [Z_{\bar{S}; \mathbf{x}_S}] \\ &= \mathbb{E}_{\mathbf{x}_{\bar{S}} \sim p(\mathbf{x}_{\bar{S}} | \mathbf{x}_S)} [Z_{\bar{S}; \mathbf{x}_S}^2] - \mathbb{E}_{\mathbf{x}_{\bar{S}} \sim p(\mathbf{x}_{\bar{S}} | \mathbf{x}_S)} [Z_{\bar{S}; \mathbf{x}_S}^2 \frac{p(\mathbf{x}_{\bar{S}} | \mathbf{x}_S)}{q(\mathbf{x}_{\bar{S}} | \mathbf{x}_S)}] \end{aligned} \quad (17)$$

As can be seen from Eq.(17), when the proposal distribution  $q(\mathbf{x}_{\bar{S}} | \mathbf{x}_S)$  is close to the true distribution  $p(\mathbf{x}_{\bar{S}} | \mathbf{x}_S)$ , the discrepancy in variance between the approximate partition function  $Z_{\bar{S}; \mathbf{x}_S}$  and the true partition function approaches zero.

### B. Dynamic masking scheme

During the training strategy, a masking scheme is used to determine whether a variable belongs to the set  $S$  or the set  $\bar{S}$ . In the traditional masking scheme, each variable is selected as the masked variable following a uniform distribution and the masked variables in set  $\bar{S}$  will continue to change with the epoch, so the model can approximate any conditional probability distribution. However, due to the choice of uniform distribution, the number of masked variables in training is always in a stable range, which limits the performance of the model.

As discussed in Ref. [27], by using a varying mask rate instead of a fixed mask rate, the model can maintain a stable performance when the input information changes. Thus, a dynamic masking rate is proposed during training to explore the probability distribution of each variable conditional on each other and further enhance the generalization ability of the model. As the epoch grows larger, the mask rate increases linearly until it reaches the set maximum mask rate. To be

specific, we set a mask rate range  $\eta \in [\eta_{min}, \eta_{max}]$ , the larger the  $\eta$ , the larger the number of masked variables. When  $v_{min} = 0$ , it means that all variables are unmasked, and  $\eta_{max} = 1$  means all variables are masked.

$$\eta_{epoch+1} = \eta_{epoch} + \Delta \quad (18)$$

where  $\Delta$  represents the increment of  $v$  after each epoch. Typically, using either all observed or all unobserved variables during model training is disallowed, as it may lead to training instability. Consequently, while establishing the dynamic mask interval, it is imperative to ensure that  $\eta_{min} > 0$ ,  $\eta_{max} < 1$ , and  $\eta_{min} < \eta_{max}$ . The detailed procedures for training EmSHAP are listed in Algorithm 1.

---

**Algorithm 1** Training procedures of EmSHAP

---

**Require:** Training data set  $\mathbf{x}$ , training epochs  $\mathcal{E}$

**Initialize:** Energy network parameters, GRU network parameters and dynamic masking scheme,  $e = 1$ .  
**while**  $e \leq \mathcal{E}$  **do**  
     $[\mathbf{x}_{\bar{S}}, \mathbf{x}_S] = \text{dynamic masking}(\mathbf{x})$   
    **for**  $j$  in  $\bar{S}$  **do**  
        GRU network( $[\mathbf{x}_{\bar{S}}, \mathbf{x}_S]$ )  $\rightarrow q(\mathbf{x}_{\bar{S}_j} | \mathbf{x}_{S \cup \bar{S}_{<j}}), \gamma$   
         $\bar{S} = \bar{S} / \{j\}$   
         $S = S \cup j$   
         $q(\mathbf{x}_{\bar{S}} | \mathbf{x}_S) = q(\mathbf{x}_{\bar{S}} | \mathbf{x}_S)q(\mathbf{x}_{\bar{S}_j} | \mathbf{x}_{S \cup \bar{S}_{<j}})$   
    **end for**  
    Sample from  $q(\mathbf{x}_{\bar{S}} | \mathbf{x}_S)$  to get  $\mathbf{x}_{\bar{S}}^{(k)}$   
    energy network( $[\mathbf{x}_{\bar{S}}^{(k)}, \mathbf{x}_S], \gamma$ )  $\rightarrow \exp(-g_{\theta}(\mathbf{x}_{\bar{S}}, \mathbf{x}_S))$   
    Calculate partition function using Eq.(9)  
    Calculate loss using Eq.(14)  
     $e = e + 1$   
**end while**

---

#### IV. ANALYSIS ON ERROR BOUND

In this section, the error bound of the contribution function in the proposed EmSHAP is discussed. It is shown in Theorem 1 that the expectation of the mean absolute deviation (MAD) between the estimated contribution function  $\hat{v}(S)$  and the true contribution function  $v(S)$  has an upper bound of  $\frac{\sqrt{\pi}}{\sqrt{2K}} + \varepsilon_1$ , where  $K$  is the number of Monte Carlo sampling,  $\varepsilon_1$  is a small positive number related to the absolute probability density ratio between the estimated conditional density and the true data-generating density. For comparison, Theorems 2 and 3 presents the error bounds of two competitive methods, i.e., KernelSHAP [12] and VAEAC [17].

To begin with, the following assumptions are introduced to facilitate the analysis.

**Assumption 1.** The parameters of the estimated conditional density  $p_{\theta}(\mathbf{x}_{\bar{S}} | \mathbf{x}_S = \mathbf{x}_S^*)$  are unbiased estimates of the parameters of the true data-generating density  $p_{data}(\mathbf{x}_{\bar{S}}^* | \mathbf{x}_S = \mathbf{x}_S^*)$ , that is, for a small positive  $\varepsilon_1$ , the probability density ratio can be described as follows,

$$\left| \frac{p_{\theta}(\mathbf{x}_{\bar{S}} | \mathbf{x}_S = \mathbf{x}_S^*)}{p_{data}(\mathbf{x}_{\bar{S}}^* | \mathbf{x}_S = \mathbf{x}_S^*)} - 1 \right| \leq \varepsilon_1 \quad (19)$$

**Assumption 2.** The predictive function  $f(\mathbf{x})$  is continuous and second-order differentiable.

**Assumption 3.** The contribution value  $v(S)$  of any subset  $S$  and the predictive value  $\hat{y} = f(\mathbf{x})$  are bounded within  $[0, 1]$ .

Assumption 1 holds as energy model can be flexibly parameterized for arbitrary probability distributions [28], [29].

Before analyzing the upper bound, the following propositions are needed to show the consistency between the Monte Carlo sampling and the asymptotic of the estimation method.

**Proposition 1.** (Consistency) From the weak law of large numbers, when the sampling time  $K$  is large enough,  $\frac{1}{K} \sum_{k=1}^K f(\mathbf{x}_{\bar{S}}^{(k)}, \mathbf{x}_S^*)$  is convergent by probability to the conditional expectation  $\mathbb{E}[f(\mathbf{x}_{\bar{S}}, \mathbf{x}_S^*) | p_{\theta}(\mathbf{x}_{\bar{S}} | \mathbf{x}_S = \mathbf{x}_S^*)]$ , that is, for any positive  $\varepsilon_2$ , we have,

$$\lim_{K \rightarrow +\infty} \mathbb{P} \left( \left| \frac{1}{K} \sum_{k=1}^K f(\mathbf{x}_{\bar{S}}^{(k)}, \mathbf{x}_S^*) - \mathbb{E}_{p_{\theta}(\mathbf{x}_{\bar{S}} | \mathbf{x}_S = \mathbf{x}_S^*)} [f(\mathbf{x}_{\bar{S}}, \mathbf{x}_S^*)] \right| \leq \varepsilon_2 \right) = 1 \quad (20)$$

**Proposition 2.** The expectation of estimated conditional density  $p_{\theta}(\mathbf{x}_{\bar{S}} | \mathbf{x}_S = \mathbf{x}_S^*)$  is convergent by probability to the expectation of true data-generating density  $p_{data}(\mathbf{x}_{\bar{S}}^* | \mathbf{x}_S = \mathbf{x}_S^*)$ , that is, for any positive  $\varepsilon_2$ , we have,

$$\mathbb{P} \left( \left| \mathbb{E}_{p_{\theta}(\mathbf{x}_{\bar{S}} | \mathbf{x}_S = \mathbf{x}_S^*)} [f(\mathbf{x}_{\bar{S}}, \mathbf{x}_S^*)] - \mathbb{E}_{p_{data}(\mathbf{x}_{\bar{S}}^* | \mathbf{x}_S = \mathbf{x}_S^*)} [f(\mathbf{x}_{\bar{S}}^*, \mathbf{x}_S^*)] \right| \leq \varepsilon_2 \right) = 1 \quad (21)$$

*Proof.* To prove Proposition 2, Taylor expansion for the expectation function is used. The absolute value of the difference between the estimated conditional expectation and the true conditional expectation is as follows.

$$\begin{aligned} & \left| \mathbb{E}_{p_{\theta}(\mathbf{x}_{\bar{S}} | \mathbf{x}_S = \mathbf{x}_S^*)} [f(\mathbf{x}_{\bar{S}}, \mathbf{x}_S^*)] - \mathbb{E}_{p_{data}(\mathbf{x}_{\bar{S}}^* | \mathbf{x}_S = \mathbf{x}_S^*)} [f(\mathbf{x}_{\bar{S}}^*, \mathbf{x}_S^*)] \right| \\ &= \left| \mathbb{E}_{p_{\theta}(\mathbf{x}_{\bar{S}} | \mathbf{x}_S = \mathbf{x}_S^*)} \left[ (f(\mathbf{x}_{\bar{S}}^*, \mathbf{x}_S^*) + f'(\mathbf{x}_{\bar{S}}^*, \mathbf{x}_S^*)(\mathbf{x}_{\bar{S}} - \mathbf{x}_{\bar{S}}^*) + o((\mathbf{x}_{\bar{S}} - \mathbf{x}_{\bar{S}}^*)^2)) \right] \right. \\ &\quad \left. - \mathbb{E}_{p_{data}(\mathbf{x}_{\bar{S}}^* | \mathbf{x}_S = \mathbf{x}_S^*)} [f(\mathbf{x}_{\bar{S}}^*, \mathbf{x}_S^*)] \right| \\ &= \left| \mathbb{E}_{p_{\theta}(\mathbf{x}_{\bar{S}} | \mathbf{x}_S = \mathbf{x}_S^*)} [f(\mathbf{x}_{\bar{S}}^*, \mathbf{x}_S^*)] - \mathbb{E}_{p_{data}(\mathbf{x}_{\bar{S}}^* | \mathbf{x}_S = \mathbf{x}_S^*)} [f(\mathbf{x}_{\bar{S}}^*, \mathbf{x}_S^*)] \right. \\ &\quad \left. + \mathbb{E}_{p_{\theta}(\mathbf{x}_{\bar{S}} | \mathbf{x}_S = \mathbf{x}_S^*)} \left[ (f'(\mathbf{x}_{\bar{S}}^*, \mathbf{x}_S^*)(\mathbf{x}_{\bar{S}} - \mathbf{x}_{\bar{S}}^*) + o((\mathbf{x}_{\bar{S}} - \mathbf{x}_{\bar{S}}^*)^2)) \right] \right| \end{aligned} \quad (22)$$

According to Assumption 1, the first term of the last equation in Eq.(22) is equal to zero, that is,  $\mathbb{E}_{p_{\theta}(\mathbf{x}_{\bar{S}} | \mathbf{x}_S = \mathbf{x}_S^*)} [f(\mathbf{x}_{\bar{S}}^*, \mathbf{x}_S^*)] - \mathbb{E}_{p_{data}(\mathbf{x}_{\bar{S}}^* | \mathbf{x}_S = \mathbf{x}_S^*)} [f(\mathbf{x}_{\bar{S}}^*, \mathbf{x}_S^*)] = 0$ . Also, since the parameters of  $p_{\theta}(\mathbf{x}_{\bar{S}} | \mathbf{x}_S = \mathbf{x}_S^*)$  are unbiased estimates of  $p_{data}(\mathbf{x}_{\bar{S}}^* | \mathbf{x}_S = \mathbf{x}_S^*)$ , we have  $\mathbb{E}[\mathbf{x}_{\bar{S}} - \mathbf{x}_{\bar{S}}^*] = 0$  and  $\mathbb{E}[o((\mathbf{x}_{\bar{S}} - \mathbf{x}_{\bar{S}}^*)^2)] = 0$ . The second term of the last equation in Eq.(22) can be negligible. Thus, Eq.(21) can be obtained.  $\square$

Proposition 1 and Proposition 2 imply the convergence of Monte Carlo sampling and the proposed energy model. Furthermore, the following corollary can be obtained.

**Corollary 1.** When the sampling number  $K$  goes to infinity, the mean of the samplings is convergence to the true conditional expectation.

$$\lim_{k \rightarrow \infty} \mathbb{P} \left( \left| \frac{1}{k} \sum_{k=1}^K f(\mathbf{x}_{\bar{S}}^{(k)}, \mathbf{x}_S^*) - \mathbb{E}_{p_{data}(\mathbf{x}_{\bar{S}}^* | \mathbf{x}_S = \mathbf{x}_S^*)} [f(\mathbf{x}_{\bar{S}}, \mathbf{x}_S^*)] \right| \geq \varepsilon_2 \right) = 1 \quad (23)$$

Thus, the larger  $K$ , the closer to the true conditional expectation, which indicates the lower bound of the difference between the estimation conditional expectation and the true conditional function is zero.

**Corollary 2.** For a small positive  $\varepsilon$ , the following inequality can be constructed,

$$\left| f(\mathbf{x}_{\bar{S}}, \mathbf{x}_S^*) \frac{p_{\theta}(\mathbf{x}_{\bar{S}} | \mathbf{x}_S = \mathbf{x}_S^*)}{p_{data}(\mathbf{x}_{\bar{S}}^* | \mathbf{x}_S = \mathbf{x}_S^*)} - f(\mathbf{x}_{\bar{S}}, \mathbf{x}_S^*) \right| \leq \varepsilon_1 \quad (24)$$

*Proof.* The proof of Corollary 2 uses Taylor expansion technique as well, which is specific as follows,

$$\begin{aligned} & \left| f(\mathbf{x}_S, \mathbf{x}_S^*) \frac{p_{\theta}(\mathbf{x}_S | \mathbf{x}_S = \mathbf{x}_S^*)}{p_{data}(\mathbf{x}_S^* | \mathbf{x}_S = \mathbf{x}_S^*)} - f(\mathbf{x}_S^*, \mathbf{x}_S^*) \right| \\ &= \left| \frac{p_{\theta}(\mathbf{x}_S | \mathbf{x}_S = \mathbf{x}_S^*)}{p_{data}(\mathbf{x}_S^* | \mathbf{x}_S = \mathbf{x}_S^*)} [f(\mathbf{x}_S^*, \mathbf{x}_S^*) + f'(\mathbf{x}_S^*, \mathbf{x}_S^*)(\mathbf{x}_{\bar{S}} - \mathbf{x}_S^*) \right. \\ & \quad \left. + o((\mathbf{x}_{\bar{S}} - \mathbf{x}_S^*)^2)] - f(\mathbf{x}_S^*, \mathbf{x}_S^*) \right| \\ &= \left| \left( \frac{p_{\theta}(\mathbf{x}_S | \mathbf{x}_S = \mathbf{x}_S^*)}{p_{data}(\mathbf{x}_S^* | \mathbf{x}_S = \mathbf{x}_S^*)} - 1 \right) f(\mathbf{x}_S^*, \mathbf{x}_S^*) \right. \\ & \quad \left. + \frac{p_{\theta}(\mathbf{x}_S | \mathbf{x}_S = \mathbf{x}_S^*)}{p_{data}(\mathbf{x}_S^* | \mathbf{x}_S = \mathbf{x}_S^*)} (f'(\mathbf{x}_S^*, \mathbf{x}_S^*)(\mathbf{x}_{\bar{S}} - \mathbf{x}_S^*) + o((\mathbf{x}_{\bar{S}} - \mathbf{x}_S^*)^2)) \right| \\ &= \left| \left( \frac{p_{\theta}(\mathbf{x}_S | \mathbf{x}_S = \mathbf{x}_S^*)}{p_{data}(\mathbf{x}_S^* | \mathbf{x}_S = \mathbf{x}_S^*)} - 1 \right) f(\mathbf{x}_S^*, \mathbf{x}_S^*) \right| \\ &= \left| \frac{p_{\theta}(\mathbf{x}_S | \mathbf{x}_S = \mathbf{x}_S^*)}{p_{data}(\mathbf{x}_S^* | \mathbf{x}_S = \mathbf{x}_S^*)} - 1 \right| \cdot |f(\mathbf{x}_S^*, \mathbf{x}_S^*)| \\ &= \varepsilon_1 f(\mathbf{x}_S^*, \mathbf{x}_S^*) \\ &\leq \varepsilon_1 \end{aligned} \quad (25)$$

According to the proof of Proposition 2,  $\mathbb{E}[\mathbf{x}_{\bar{S}} - \mathbf{x}_S^*] = 0$  and  $\mathbb{E}[o((\mathbf{x}_{\bar{S}} - \mathbf{x}_S^*)^2)] = 0$ , thus,

$$\frac{p_{\theta}(\mathbf{x}_S | \mathbf{x}_S = \mathbf{x}_S^*)}{p_{data}(\mathbf{x}_S^* | \mathbf{x}_S = \mathbf{x}_S^*)} (f'(\mathbf{x}_S^*, \mathbf{x}_S^*)(\mathbf{x}_{\bar{S}} - \mathbf{x}_S^*) + o((\mathbf{x}_{\bar{S}} - \mathbf{x}_S^*)^2)) = 0 \quad (26)$$

Also, refer to Assumption 3,  $f(\mathbf{x}_S^*, \mathbf{x}_S^*)$  is bounded with  $[0, 1]$ , Eq.(24) can be obtained.  $\square$

**Lemma 1.** (Hoeffding's inequality) [30] Let  $u_1, \dots, u_K$  be i.i.d. random variables such that  $a \leq u_k \leq b$ . Then for any  $\varepsilon_2 > 0$ ,

$$\mathbb{P} \left( \left| \frac{1}{K} \sum_{k=1}^K (u_k - \mathbb{E}[u_k]) \right| \geq \varepsilon_2 \right) \leq 2 \exp \left( - \frac{2K\varepsilon_2^2}{(b-a)^2} \right) \quad (27)$$

Hoeffding's inequality is an important technique for establishing upper bounds on the probability of sums involving bounded random variables deviating significantly from their expected values. By using Lemma 1, the following corollary is obtained.

**Corollary 3.** (corollary of Hoeffding's inequality) For all  $\varepsilon > 0$ , we have,

$$\begin{aligned} & \mathbb{P} \left( \left| \frac{1}{K} \sum_{k=1}^K f(\mathbf{x}_{\bar{S}}^{(k)}, \mathbf{x}_S^*) - \mathbb{E}_{p_{\theta}(\mathbf{x}_{\bar{S}} | \mathbf{x}_S = \mathbf{x}_S^*)} [f(\mathbf{x}_{\bar{S}}, \mathbf{x}_S^*)] \right| \geq \varepsilon_2 \right) \\ & \leq 2 \exp \left( -2K\varepsilon_2^2 \right) \end{aligned} \quad (28)$$

*Proof.* Since the predictive value is bounded within  $[0, 1]$  according to Assumption 3, by applying Hoeffding's inequality, we can get

$$\begin{aligned} & \mathbb{P} \left( \left| \frac{1}{K} \sum_{k=1}^K \left( f(\mathbf{x}_{\bar{S}}^{(k)}, \mathbf{x}_S^*) - \mathbb{E}_{p_{\theta}(\mathbf{x}_{\bar{S}} | \mathbf{x}_S = \mathbf{x}_S^*)} [f(\mathbf{x}_{\bar{S}}, \mathbf{x}_S^*)] \right) \right| \geq \varepsilon_2 \right) \\ &= \mathbb{P} \left( \left| \frac{1}{K} \sum_{k=1}^K f(\mathbf{x}_{\bar{S}}^{(k)}, \mathbf{x}_S^*) - \frac{1}{K} \sum_{k=1}^K \mathbb{E}_{p_{\theta}(\mathbf{x}_{\bar{S}} | \mathbf{x}_S = \mathbf{x}_S^*)} [f(\mathbf{x}_{\bar{S}}^{(k)}, \mathbf{x}_S^*)] \right| \geq \varepsilon_2 \right) \\ &\leq 2 \exp \left( -2K\varepsilon_2^2 \right) \end{aligned} \quad (29)$$

$\mathbf{x}_{\bar{S}}^{(k)}$  is sampled from  $p_{\theta}(\mathbf{x}_{\bar{S}} | \mathbf{x}_S = \mathbf{x}_S^*)$  and the expectation of  $f(\mathbf{x}_{\bar{S}}^{(k)}, \mathbf{x}_S^*)$  is equal to  $\mathbb{E}_{p_{\theta}(\mathbf{x}_{\bar{S}} | \mathbf{x}_S = \mathbf{x}_S^*)} [f(\mathbf{x}_{\bar{S}}, \mathbf{x}_S^*)]$  for any sample. Thus, Eq.(28) is obtained.  $\square$

By the propositions and corollaries discussed above, the upper bound of the expectation between the mean absolute deviation between the estimation contribution function  $\hat{v}(S)$  and the true contribution function  $v(S)$  can be calculated as follows.

**Theorem 1.** (EmSHAP estimation error upper bound) The expectation of the mean absolute deviation (MAD) between the estimation contribution function  $\hat{v}(S)$  and the true contribution function  $v(S)$  is upper bounded with  $\frac{\sqrt{\pi}}{\sqrt{2K}} + \varepsilon$ , where  $K$  is the sampling number and  $\varepsilon$  is a small positive number.

*Proof.*  $\mathbb{E}[|\hat{v}(S) - v(S)|]$  can be decomposed into two parts, namely the approximation error and the statistic error. The detailed derivation is given as follows.

$$\begin{aligned} & \mathbb{E}[|\hat{v}(S) - v(S)|] \\ &= \mathbb{E} \left[ \left| \frac{1}{K} \sum_{k=1}^K f(\mathbf{x}_{\bar{S}}^{(k)}, \mathbf{x}_S^*) - \mathbb{E}_{p_{data}(\mathbf{x}_{\bar{S}} | \mathbf{x}_S = \mathbf{x}_S^*)} [f(\mathbf{x}_{\bar{S}}, \mathbf{x}_S^*)] \right| \right] \\ &= \mathbb{E} \left[ \left| \frac{1}{K} \sum_{k=1}^K f(\mathbf{x}_{\bar{S}}^{(k)}, \mathbf{x}_S^*) - \mathbb{E}_{p_{\theta}(\mathbf{x}_{\bar{S}} | \mathbf{x}_S = \mathbf{x}_S^*)} [f(\mathbf{x}_{\bar{S}}, \mathbf{x}_S^*)] \right. \right. \\ & \quad \left. \left. + \mathbb{E}_{p_{\theta}(\mathbf{x}_{\bar{S}} | \mathbf{x}_S = \mathbf{x}_S^*)} [f(\mathbf{x}_{\bar{S}}, \mathbf{x}_S^*)] - \mathbb{E}_{p_{data}(\mathbf{x}_{\bar{S}} | \mathbf{x}_S = \mathbf{x}_S^*)} [f(\mathbf{x}_{\bar{S}}, \mathbf{x}_S^*)] \right| \right] \\ &\leq \mathbb{E} \left[ \left| \frac{1}{K} \sum_{k=1}^K f(\mathbf{x}_{\bar{S}}^{(k)}, \mathbf{x}_S^*) - \mathbb{E}_{p_{\theta}(\mathbf{x}_{\bar{S}} | \mathbf{x}_S = \mathbf{x}_S^*)} [f(\mathbf{x}_{\bar{S}}, \mathbf{x}_S^*)] \right| \right] \\ & \quad + \mathbb{E} \left[ \left| \mathbb{E}_{p_{\theta}(\mathbf{x}_{\bar{S}} | \mathbf{x}_S = \mathbf{x}_S^*)} [f(\mathbf{x}_{\bar{S}}, \mathbf{x}_S^*)] - \mathbb{E}_{p_{data}(\mathbf{x}_{\bar{S}} | \mathbf{x}_S = \mathbf{x}_S^*)} [f(\mathbf{x}_{\bar{S}}, \mathbf{x}_S^*)] \right| \right] \end{aligned} \quad (30)$$

where  $\mathbf{x}_{\bar{S}} \sim p_{\theta}(\mathbf{x}_{\bar{S}} | \mathbf{x}_S = \mathbf{x}_S^*)$ . The first term in the last inequality of Eq.(30) is the approximation error and the second is the statistical error. The upper bound of the approximation error

is first considered.

$$\begin{aligned}
& \mathbb{E} \left[ \left| \frac{1}{k} \sum_{k=1}^K f(\mathbf{x}_{\bar{S}}^{(k)}, \mathbf{x}_S^*) - \mathbb{E}_{p_\theta(\mathbf{x}_{\bar{S}}|\mathbf{x}_S=\mathbf{x}_S^*)} [f(\mathbf{x}_{\bar{S}}, \mathbf{x}_S^*)] \right| \right] \\
&= 2 \mathbb{E} \left[ \left( \frac{1}{k} \sum_{k=1}^K f(\mathbf{x}_{\bar{S}}^{(k)}, \mathbf{x}_S^*) - \mathbb{E}_{p_\theta(\mathbf{x}_{\bar{S}}|\mathbf{x}_S=\mathbf{x}_S^*)} [f(\mathbf{x}_{\bar{S}}, \mathbf{x}_S^*)] \right)_+ \right] \\
&= 2 \int_0^{+\infty} \mathbb{P} \left( \frac{1}{k} \sum_{k=1}^K f(\mathbf{x}_{\bar{S}}^{(k)}, \mathbf{x}_S^*) - \mathbb{E}_{p_\theta(\mathbf{x}_{\bar{S}}|\mathbf{x}_S=\mathbf{x}_S^*)} [f(\mathbf{x}_{\bar{S}}, \mathbf{x}_S^*)] \geq \varepsilon_2 \right) d\varepsilon_2 \\
&\leq 2 \int_0^{+\infty} \exp(-2K\varepsilon_2^2) d\varepsilon_2 \\
&= \frac{\sqrt{\pi}}{\sqrt{2K}}
\end{aligned} \tag{31}$$

where  $(\cdot)_+$  is  $\max(\cdot, 0)$ , the integral in Eq.(31) uses the formula  $\mathbb{E}[u] = \int_0^{+\infty} \mathbb{P}(u > \varepsilon) d\varepsilon$  for a non-negative random variable  $u$ , the inequality in Eq.(31) uses the corollary discussed in Corollary 3. Hence, the approximate error is bounded by  $\frac{\sqrt{\pi}}{\sqrt{2K}}$ . The derivation of the statistical error is given as follows.

$$\begin{aligned}
& \mathbb{E} \left[ \left| \mathbb{E}_{p_\theta(\mathbf{x}_{\bar{S}}|\mathbf{x}_S=\mathbf{x}_S^*)} [f(\mathbf{x}_{\bar{S}}, \mathbf{x}_S^*)] - \mathbb{E}_{p_{data}(\mathbf{x}_{\bar{S}}|\mathbf{x}_S=\mathbf{x}_S^*)} [f(\mathbf{x}_{\bar{S}}, \mathbf{x}_S^*)] \right| \right] \\
&= \mathbb{E} \left[ \left| \int f(\mathbf{x}_{\bar{S}}, \mathbf{x}_S^*) p_\theta(\mathbf{x}_{\bar{S}}|\mathbf{x}_S=\mathbf{x}_S^*) d\mathbf{x}_{\bar{S}} - \int f(\mathbf{x}_{\bar{S}}, \mathbf{x}_S^*) p_{data}(\mathbf{x}_{\bar{S}}|\mathbf{x}_S=\mathbf{x}_S^*) d\mathbf{x}_{\bar{S}} \right| \right] \\
&= \mathbb{E} \left[ \left| \int f(\mathbf{x}_{\bar{S}}, \mathbf{x}_S^*) \frac{p_\theta(\mathbf{x}_{\bar{S}}|\mathbf{x}_S=\mathbf{x}_S^*)}{p_{data}(\mathbf{x}_{\bar{S}}|\mathbf{x}_S=\mathbf{x}_S^*)} p_{data}(\mathbf{x}_{\bar{S}}|\mathbf{x}_S=\mathbf{x}_S^*) d\mathbf{x}_{\bar{S}} - \int f(\mathbf{x}_{\bar{S}}, \mathbf{x}_S^*) p_{data}(\mathbf{x}_{\bar{S}}|\mathbf{x}_S=\mathbf{x}_S^*) d\mathbf{x}_{\bar{S}} \right| \right] \\
&= \mathbb{E} \left[ \left| \mathbb{E}_{p_{data}(\mathbf{x}_{\bar{S}}|\mathbf{x}_S=\mathbf{x}_S^*)} \left[ \left( f(\mathbf{x}_{\bar{S}}, \mathbf{x}_S^*) \frac{p_\theta(\mathbf{x}_{\bar{S}}|\mathbf{x}_S=\mathbf{x}_S^*)}{p_{data}(\mathbf{x}_{\bar{S}}|\mathbf{x}_S=\mathbf{x}_S^*)} - f(\mathbf{x}_{\bar{S}}, \mathbf{x}_S^*) \right) \right] \right| \right] \\
&\leq \mathbb{E} \left[ \left| \mathbb{E}_{p_{data}(\mathbf{x}_{\bar{S}}|\mathbf{x}_S=\mathbf{x}_S^*)} \left[ f(\mathbf{x}_{\bar{S}}, \mathbf{x}_S^*) \frac{p_\theta(\mathbf{x}_{\bar{S}}|\mathbf{x}_S=\mathbf{x}_S^*)}{p_{data}(\mathbf{x}_{\bar{S}}|\mathbf{x}_S=\mathbf{x}_S^*)} - f(\mathbf{x}_{\bar{S}}, \mathbf{x}_S^*) \right] \right| \right] \\
&= \varepsilon_1
\end{aligned} \tag{32}$$

By combining Eq.(31) and Eq.(32), the upper bound of  $\mathbb{E}[\|\hat{v}(S) - v(S)\|]$  can be obtained, which is  $\frac{\sqrt{\pi}}{\sqrt{2K}} + \varepsilon_1$ .  $\square$

We now discuss the tightness of the upper bound for the contribution function estimation error. The first inequality used is the triangle inequality for absolute values in Eq.(30). If the two functions on the right side of the inequality share the same sign (both positive or negative), that is,

$$\left( \frac{1}{k} \sum_{k=1}^K f(\mathbf{x}_{\bar{S}}^{(k)}, \mathbf{x}_S^*) - \mathbb{E}_{p_\theta(\mathbf{x}_{\bar{S}}|\mathbf{x}_S=\mathbf{x}_S^*)} [f(\mathbf{x}_{\bar{S}}, \mathbf{x}_S^*)] \right) \cdot$$

$$\left( \mathbb{E}_{p_\theta(\mathbf{x}_{\bar{S}}|\mathbf{x}_S=\mathbf{x}_S^*)} [f(\mathbf{x}_{\bar{S}}, \mathbf{x}_S^*)] - \mathbb{E}_{p_{data}(\mathbf{x}_{\bar{S}}|\mathbf{x}_S=\mathbf{x}_S^*)} [f(\mathbf{x}_{\bar{S}}, \mathbf{x}_S^*)] \right) \geq 0$$

the bound derived from applying the absolute value triangle inequality is tight. Another inequality is the expectation inequality of absolute values in Eq.(32). This inequality shows that when the variable always has the same sign, which means,

$$\begin{aligned}
& \sum_{\mathbf{x}_{\bar{S}}} f(\mathbf{x}_{\bar{S}}, \mathbf{x}_S^*) \frac{p_\theta(\mathbf{x}_{\bar{S}}|\mathbf{x}_S=\mathbf{x}_S^*)}{p_{data}(\mathbf{x}_{\bar{S}}|\mathbf{x}_S=\mathbf{x}_S^*)} - f(\mathbf{x}_{\bar{S}}, \mathbf{x}_S^*) \\
&= \sum_{\mathbf{x}_{\bar{S}}} \left| f(\mathbf{x}_{\bar{S}}, \mathbf{x}_S^*) \frac{p_\theta(\mathbf{x}_{\bar{S}}|\mathbf{x}_S=\mathbf{x}_S^*)}{p_{data}(\mathbf{x}_{\bar{S}}|\mathbf{x}_S=\mathbf{x}_S^*)} - f(\mathbf{x}_{\bar{S}}, \mathbf{x}_S^*) \right|
\end{aligned} \tag{34}$$

Hence, if  $\mathbf{x}_{\bar{S}}$  satisfies both Eqs.(33) and (34), the upper bound is tight.

**Theorem 2.** (*KernelSHAP estimation error upper bound*) For any fixed  $|D|$  and when the sampling number  $K$  goes to positive infinity, under the probability greater than  $1 - 2((|D|+1)^2 + (|D|+1)) \exp(-2K\varepsilon_2^2)$ , the expectation of the mean absolute deviation (MAD) between the estimation contribution function  $\hat{v}(S)$  estimated by KernelSHAP [12] and the true contribution function  $v(S)$  is upper bounded with,

$$\begin{aligned}
& \mathbb{E}[\|\hat{v}(S) - v(S)\|] \\
&\leq 2(|D|+1) \frac{\sqrt{\pi}}{\sqrt{2K}} \|\Sigma^{*-1}\|_F + 2(|D|+1)^{\frac{5}{2}} \frac{\sqrt{\pi}}{\sqrt{2K}} \|\Sigma^{*-1}\|_F^2 + \varepsilon_2^2
\end{aligned} \tag{35}$$

where  $\varepsilon_2$  is a small positive number.  $\Sigma^* \in \mathbb{R}^{K \times K}$  is the expectation of Shapley kernel symmetric matrix, more detail information about this matrix can be found in Ref. [12].

*Proof.* The detailed proof can be found in Appendix.A.  $\square$

**Theorem 3.** (*VAEAC estimation error upper bound*) The expectation of the mean absolute deviation (MAD) between the estimation contribution function  $\hat{v}(S)$  estimated by VAEAC [17] and the true contribution function  $v(S)$  is upper bounded with  $\frac{\sqrt{\pi}}{\sqrt{2K}} + \varepsilon_1 + \delta$ , where  $K$  is the sampling number,  $\varepsilon_1$  is the probability density ratio between the estimation conditional probability  $p_\theta(\mathbf{x}_{\bar{S}}|\mathbf{x}_S=\mathbf{x}_S^*)$  and the optimal conditional probability  $p_{\theta^*}(\mathbf{x}_{\bar{S}}|\mathbf{x}_S=\mathbf{x}_S^*)$  estimated using VAE,  $\delta$  is a positive number related to KL divergence in VAE.

$$\left| \frac{p_{\theta^*}(\mathbf{x}_{\bar{S}}|\mathbf{x}_S=\mathbf{x}_S^*)}{p_{data}(\mathbf{x}_{\bar{S}}|\mathbf{x}_S=\mathbf{x}_S^*)} - 1 \right| \leq \delta \tag{36}$$

*Proof.* The detailed proof can be found in Appendix.B.  $\square$

Theorems 2 and 3 analyzed the error bounds of two widely applied methods of KernelSHAP [12] and VAEAC [17]. Theorem 2 shows that as the sampling time  $K$  increases, the first term of the right hand side of Eq.(35) vanishes, hence its error bound is governed by the second term. Since  $\|\Sigma^{*-1}\|_F^2$  is a constant, it can be seen that the error bound of KernelSHAP is highly related to the dimension of input features  $D$ . That is to say, the estimation accuracy will decrease with the input feature dimension increases. On the other hand, comparing Theorem 1 and Theorem 3 it can be seen that the error bound of VAEAC is greater than the energy model as  $\delta$  is always greater than zero. Hence it can be concluded that the proposed energy model-based Shapley value estimation method has more tight error bound than KernelSHAP and VAEAC.

## V. CASE STUDIES

### A. Application to a medical example

In this subsection, the diabetes data set (available from <https://www4.stat.ncsu.edu/boos/var.select/diabetes.html>) is considered [31] to test the performance of EmSHAP, which has been widely used in testing of XAI methods [18], [32]. The diabetes data set consists of data collected from 442 patients, involving 10 input features including age, sex, body mass index (BMI), average blood pressure, six blood serum

measurements ( $x_1, x_2, \dots, x_{10}$ ) and a continuous output ( $y$ ) related to the progression of diabetes measured in the time range of one year after baseline feature assessment, a more detailed data description can be referred to [31].

The purpose here is to establish a deep learning model to predict the diabetes measured one year after baseline using the 10 input features. Here, the stacked denoising autoencoder (SDAE) [33] is used to map the input features onto a latent space by stacking multiple denoising autoencoders (DAEs), the latent features are then fed into a fully connected layer to estimate the diabetes. The stacked DAEs can reduce error propagation and extract more information from the input features. In this application, a total of two denoising autoencoders are stacked and the noise term is set as 0.01, with the dimensions of latent space being 6 and 4, respectively. The first 300 samples are used as the training set, and samples 301~442 are allocated to the test set. Fig. 4 illustrates the predictive results of the SDAE model, with the red line corresponding to model predictions and the black line the actual disease progression. The SDAE model yields a root mean square error (RMSE) of 0.1641 and a R-squared ( $R^2$ ) value of 0.51, indicating an acceptable predictive performance.

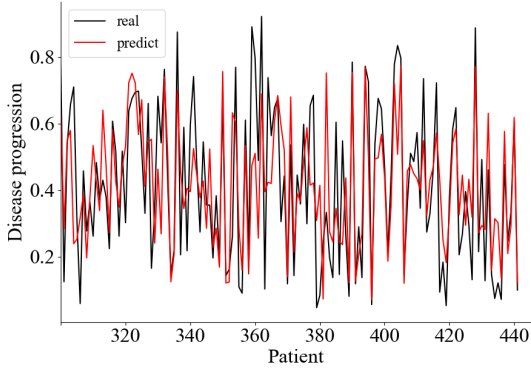


Fig. 4. SDAE prediction result

Given that SDAE is a black-box model, it is difficult to understand the importance of different input features. In order to perform this task, EmSHAP is employed to quantify the influence of input features to the predictive results. For comparison, the exact Shapley value estimation method [11], KernelSHAP [12] and VAEAC method [17] are considered.

For EmSHAP, a four-layer fully connected network with residual connections is used as the energy network. Each fully-connected layer in the energy network has a size of 128. On the other hand, the proposed network incorporates a GRU unit with output dimension of 64 and the context vector size is set as 32. To ensure comprehensive coverage of the real data distribution, the number of labels for Gaussian mixture model is set as 10. For dynamic masking, the minimum and maximum thresholds are set as  $\eta_{min} = 0.2$  and  $\eta_{max} = 0.8$ , respectively. The EmSHAP is trained and utilized to estimate the conditional probability distributions of the test data, which are further used to estimate the Shapley value. The training

epochs and sampling number for both VAEAC and EmSHAP are set as 300 and 20, respectively.

For better illustration of the estimation accuracy, Figure 5 presents the results of a total of four estimation cases, involving histograms of the estimated local Shapley values for samples Nos. of 374, 394 and 429 as well as the average absolute values of all test samples. Upon analyzing the training data, the average predictive value of all the training samples is  $\phi_0 = \mathbb{E}[f(\mathbf{x})] = 0.385$ . Sample No. 374 has a predictive value of  $\hat{y}_{374} = 0.391$ , which is close to  $\phi_0$ , whilst sample Nos. 397 and 429 have predictive values of 0.070 and 0.772, corresponding to the cases of below and above average predictions. From Figure 5 it can be seen that Sample No. 374 has a mixture of negative and positive Shapley values, while No. 397 has mostly negative values and No. 429 mostly positive values. This indicates when the predictive value of a sample falls below the average, the Shapley values of the input features are predominantly negative. Conversely, when the predictive value of a sample exceeds the average predictive value, the Shapley values of the input features are predominantly positive. A more delicate observation on the first and fourth plot of Figure 5 indicates that  $x_2, x_3$  and  $x_9$  has the most significant Shapley values, indicating they have the highest contribution to the model. For the second plot, it can be seen that the low predictive value is mostly contributed by  $x_2, x_3$  and  $x_9$ ; whilst the third plot shows that the high predictive value is mostly caused by  $x_3, x_4$  and  $x_9$ .

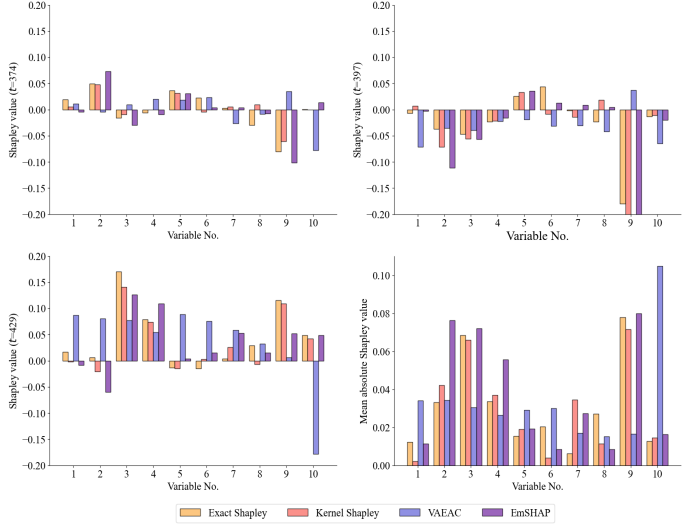


Fig. 5. Shapley value histograms of three typical samples and the average absolute Shapley value for the training samples based on SDAE

For comparison of estimation accuracy, Figure 5 illustrates that estimated values of KernelSHAP and EmSHAP are closer to the exact Shapley values. On the other hand, the accuracies VAEAC yields are not stable and may yield very bad estimations, especially for  $x_{10}$ . This result is anticipated because VAEAC characterizes the hidden space through a unimodal Gaussian distribution, which is not in line with practical situations. For a more comprehensive representation of the Shapley values across all test samples, Figure 6 displays the

Shapley probability density estimations for all input features by different methods.

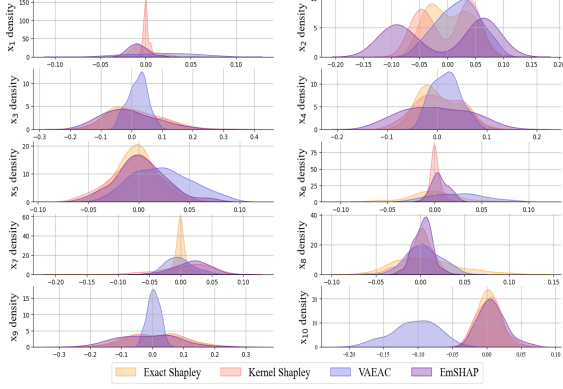


Fig. 6. Shapley probability density estimations for all input features by different methods for SDAE

In Fig. 6, the probability density curve estimated by EmSHAP closely aligns with the probability density curve of the exact Shapley value for the majority of variables. In contrast, the KernelSHAP and VAEAC methods exhibit varying degrees of deviation. To provide a meticulous assessment of the performance of different methods, this paper introduces two criteria for evaluating the disparities between these methods and the exact Shapley values. Specifically, the mean absolute error (MAE) [17] and the 2-Wasserstein distance [34] are employed.

$$CR_1 = MAE_\phi = \frac{1}{n_{test}} \frac{1}{|D|} \sum_{t=1}^{n_{test}} \sum_{i=1}^{|D|} |\phi_{i,exact}(\mathbf{x}_t) - \phi_{i,method}(\mathbf{x}_t)| \quad (37)$$

$$CR_2 = \mathcal{W}_\phi^2 = \frac{1}{|D|} \sum_{i=1}^{|D|} \mathcal{W}^2(p(\phi_{i,exact}), p(\phi_{i,method})) \quad (38)$$

$$= \frac{1}{|D|} \sum_{i=1}^{|D|} \inf_{\substack{X \sim p(\phi_{i,exact}) \\ Y \sim p(\phi_{i,method})}} (\mathbb{E} \|X - Y\|^2)$$

Here,  $CR_1$  calculates the sum of differences between the Shapley values and the exact Shapley values for each sample point across all variables.  $CR_2$ , on the other hand, assesses the difference between Shapley value distribution and the exact Shapley value distribution. Smaller outcomes obtained from these two evaluation indices indicate a more accurate Shapley value estimation. The results of both evaluation indices are presented in Table I. From Table I one can observe that EmSHAP and KernelSHAP have close  $CR_1$  and  $CR_2$  values, which are both significantly smaller than that of VAEAC. This further indicates the effectiveness of the proposed method.

TABLE I  
CRITERIA OF INTERPRETING THE SDAE PREDICTION MODEL USING THREE ESTIMATION METHODS

Criteria	Method		
	KernelSHAP	VAEAC	EmSHAP
$CR_1$	1.59E-2	5.48E-2	2.31E-2
$CR_2$	1.36E-3	4.50E-3	0.86E-3

In practical application, computation efficiency is another significant concern. in this experiment, a workstation equipped with an Intel Xeon Gold 6326 processor, 377G memory and RTX 4080 graphics processing unit was used. The calculations were performed using Python 3.9 and Tensorflow 2.9.0. The calculation time for these methods are compared and listed in Table II. Exact Shapley and KernelSHAP do not require training, but they require longer computation times during the test phase. EmSHAP and VAEAC need to train the model parameters in advance. After the training is completed, the calculation efficiency in the test phase is higher than the other methods. It should be noted that although EmSHAP has longer training and test time, its estimation accuracy is much better than VAEAC.

TABLE II  
COMPARISON OF CALCULATION TIME FOR DIFFERENT METHODS

Phase	Method			
	Exact Shapley	KernelSHAP	VAEAC	EmSHAP
Training	/	/	274.44s	369.32s
Test	743.24s	2062.44s	78.54s	197.73s

After obtaining the Shapley value for each variable, the one exhibiting a greater mean absolute Shapley value is expected to make a more substantial contribution to the SDAE. These variables are key variables in SDAE prediction model, such as  $x_3$ ,  $x_9$ . The absence of these key variables during prediction significantly diminishes the model performance. In other words, the SDAE primarily relies on the body mass index (bmi) and possibly log of serum triglycerides level (ltg) as key features to predict diabetes. To substantiate this assertion, we mask each of the 10 features in order and input the masked data into the SDAE model for prediction. The results are presented in Table III.

TABLE III  
MASKED VARIABLES AND PREDICTION ACCURACY OF SDAE AFTER MASKING

Masked No.	RMSE	Masked No.	RMSE
$x_1$	0.1667	$x_6$	0.1707
$x_2$	0.1711	$x_7$	0.1909
$x_3$	0.2556	$x_8$	0.1647
$x_4$	0.2144	$x_9$	0.3380
$x_5$	0.1744	$x_{10}$	0.1777

Table III provides a clear view of the change in prediction accuracies after masking each input feature. It can be seen that the sharpest increase in RMSE is observed by masking  $x_9$ , followed by  $x_3$  and  $x_4$ . Conversely, when  $x_1$  is masked,

there is negligible change in the predictive performance. These results align with the Shapley value-based results, affirming the credibility of the model's interpretability analysis rooted in the Shapley value.

Furthermore, the proposed method encompasses the original energy model, GRU coupling, and a dynamic masking mechanism. We conducted an ablation experiment analysis on this approach to demonstrate that the combination of these three strategies continues to ensure the model performance. Figure 7 presents the loss curves, energy probability density maximum likelihood curves, and proposal probability density maximum likelihood curves for four different model structures during training: the original energy network, the energy network with the dynamic mask mechanism, the energy network coupled with GRU, and the proposed method. Each point corresponding to an epoch represents the mean value of all batch loss functions, energy maximum likelihood, and proposal maximum likelihood for that epoch.

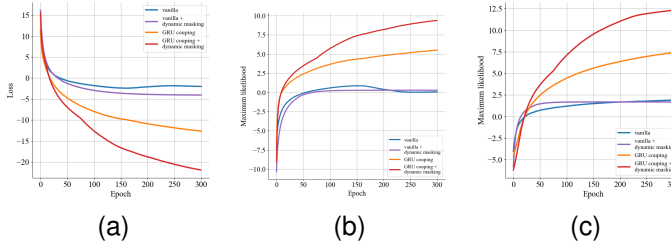


Fig. 7. The loss, energy distribution maximum likelihood, and proposal distribution maximum likelihood in model training

It can be seen from the figure that the maximum likelihood values of the energy network and the proposed network will be greatly improved when GRU (yellow curve) is introduced into the original model (blue curve), while the model with only dynamic mask scheme (purple curve) does not show much improvement in the results. In contrast, the proposed method (red curve) demonstrates the highest maximum likelihood estimate, affirming its superior ability to accurately estimate arbitrary conditional probability distributions, this is consistent with the analysis presented in Section V.

### B. Application to an industrial example

This subsection investigates the performance of EmSHAP for explaining deep learning model for an industrial example involving prediction of water wall temperature of a boiler. The water wall is a crucial component of the boiler system, consisting of neatly arranged metal tubes positioned close to the furnace interior. Water running in the water wall tube absorbs the radiant heat from the high-temperature flame within the furnace, producing steam for electricity generation. The water wall tube has a temperature limit due to its material characteristics, prolonged operation above the limit may lead to serious accident of tube burst. Hence it is important to predict the future temperature of water wall tubes so that corrective operations can be performed to ensure safety. In this case, operational data collected from an industrial boiler of a

coal-fired power plant in Northeastern China is considered. For this application, a total of 8 input features are considered and listed in Table IV, and the output relates to the temperature of tube No. 1. This data set consists of 4500 samples, with the first 3000 being the training data and the remaining 1500 as the test data. The sampling time for this data set is 15s. And the purpose is to predict the temperature of tube No. 1 10 minutes from the current time.

TABLE IV  
PROCESS VARIABLES AND DESCRIPTIONS

No.	Description	No.	Description
$x_1$	Total fuel	$x_5$	Water to coal ratio
$x_2$	Total water flow	$x_6$	Main steam temperature
$x_3$	Total airflow	$x_7$	Boiler load
$x_4$	Boiler feed water temperature	$x_8$	Furnace pressure

This time, another deep learning model—the multidimensional convolutional neural network (MDCNN) [35] is used. In the MDCNN model, input features are fed into both one-dimensional CNN (1DCNN) and two-dimensional CNN (2DCNN) for the extraction of input information, which are further concatenated and passed through a fully connected layer to generate the predictive values. Here, both 1DCNN and 2DCNN involve convolution of two layers. The convolution kernel sizes for the two layer are 5 and 3. The output of each convolution layer is connected to the maximum pooling layer and the sizes of the maximum pooling layers are all set as 3. The model is optimized using the Adam optimizer with a learning rate of 0.01. Figure 8 shows the predictive results obtained using MDCNN.

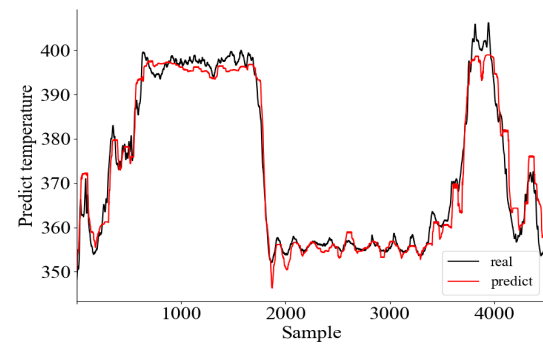


Fig. 8. Predictive

The RMSE and  $R^2$  yielded by the MDCNN model are 4.40 and 0.92, indicating a good predictive performance. Again, four methods are used to quantify the contribution of input features to the MDCNN model. The hyperparameters of VAEAC and EmSHAP are the same as Section V-A. The average predictive value for temperature 10 minutes later for the training data is  $\phi_0 = \mathbb{E}[f(\mathbf{x})] = 374.33^\circ\text{C}$ . Similar to Section V-A, the Shapley value histogram for three individual predictions of  $\hat{y}_{3050} = 356.32^\circ\text{C}$ ,  $\hat{y}_{3715} = 380.23^\circ\text{C}$ , and  $\hat{y}_{4000} = 395.93^\circ\text{C}$  and the average absolute values of the test data are shown in Fig. 9. This time, Fig. 9 shows that at  $t = 3050$ , the input features have a mixture of positive and negative Shapley values, and the most

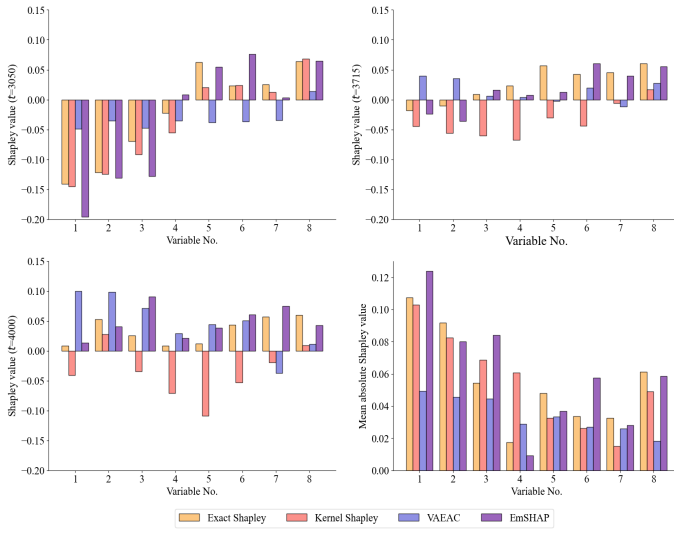


Fig. 9. Shapley value histograms of three typical samples and mean absolute for the test data based on MDCNN

significant contributions are from  $x_1$ ,  $x_2$ , and  $x_3$ . In contrast, when the predictive value is close to and above the average, most of the Shapley values are positive, as is indicated by the second and third plot. Comparing the second and third plot it can be seen that the most significant change is observed for  $x_2$ , which indicates that change in  $x_2$  is most responsible for the increase in predictive value.

A closer look at Fig.9 shows that KernelSHAP yields negative values whilst the true values are positive. This can be explained, as KernelSHAP assume independence among input features. For this case, however, the input variables have high correlation. To provide a more comprehensive illustration of the Shapley values obtained through different methods, Fig. 10 displays the distribution of Shapley values for each variable across all test samples.

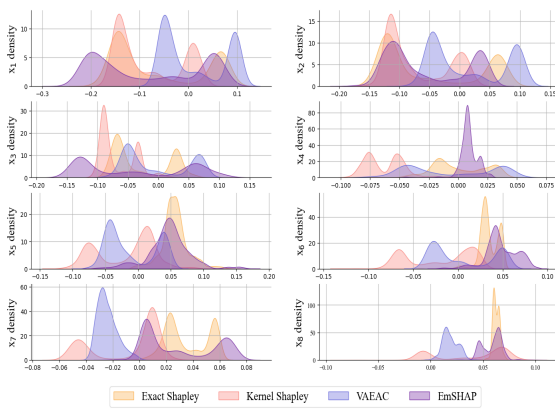


Fig. 10. Shapley probability density estimations for all input features by different methods for MDCNN

In Fig. 10, it can be found that the probability density curves of EmSHAP and the exact Shapley value method have a high degree of agreement. However, the estimation methods of KernelSHAP and VAEAC have relatively low agreement with the

exact Shapley value method. This can be explained, because KernelSHAP does not consider the conditional correlation between variables, resulting in a deviation in the calculated Shapley value. VAEAC uses unimodal Gaussian distribution to describe latent space information, and its generalization and robustness are weaker than energy models, leading to higher estimation bias. On the contrary, EmSHAP can accurately estimate the Shapley value on most of the variables. Table V shows the mean absolute error and the 2-Wasserstein distance for each estimation method in comparison to the exact Shapley values. As shown in Table V, EmSHAP has a lower MAE compared to the other two methods in Shapley value estimation. Additionally, the Wasserstein distance of the estimated Shapley value distribution is lower, which also means that estimation is in closer proximity to the exact Shapley value.

TABLE V  
CRITERIA OF INTERPRETING THE MDCNN USING DIFFERENT ESTIMATION METHODS

Criteria	Method		
	KernelSHAP	VAEAC	EmSHAP
$CR_1$	4.43E-2	4.92E-2	2.28E-2
$CR_2$	2.02E-3	2.06E-3	6.02E-4

For computational efficiency, the same hardware and software configurations to Section V-A are used. The calculation time are listed in Table VI. It can be observed that in the test phase, VAEAC and EmSHAP have the shortest calculation time of 152.90s and 188.64s. On the other hand, the calculation time for Exact Shapley and KernelSHAP are 2156.78s and 6538.82s, which is much higher than those of VAEAC and EmSHAP.

TABLE VI  
COMPARISON OF CALCULATION TIME

Phase	Method			
	Exact Shapley	KernelSHAP	VAEAC	EmSHAP
Training	/	/	1814.99s	1951.43s
Test	2156.78s	6538.82s	152.90s	188.64s

To verify that variables with large Shapley values have a greater contribution in the MDCNN model, each variable is masked in order, and the masked data is fed into MDCNN for prediction. The resulting predictive accuracies for the masked variables are listed in Table VII.

TABLE VII  
MASKED VARIABLES AND PREDICTION ACCURACY OF MDCNN AFTER MASKING

Masked No.	RMSE	Masked No.	RMSE
$x_1$	9.18	$x_5$	5.44
$x_2$	8.79	$x_6$	4.62
$x_3$	5.43	$x_7$	4.51
$x_4$	4.48	$x_8$	7.48

It can be seen from Table VII that after  $x_1$  and  $x_2$  are masked, the predictive accuracies exhibit a substantial decrease. Specifically, when  $x_1$  is masked, RMSE increases to

9.18. This indicates a substantial decline in MDCNN predictive performance when  $x_1$  is omitted. Conversely, when  $x_4$ ,  $x_6$ , and  $x_7$  are masked, the RMSE values do not show much change. The results in Table VII is in accordance with the results in Fig. 9. This further confirms the reliability of the results obtained through EmSHAP.

Moreover, the ablation experiment analysis of EmSHAP in this case is also discussed here. Figure 11 displays the loss curves, energy probability density maximum likelihood curves, and proposal probability density maximum likelihood curves for four different energy-based model structures during training: the original energy network, the energy network with dynamic mask scheme, the energy network coupled with GRU, and the proposed method.

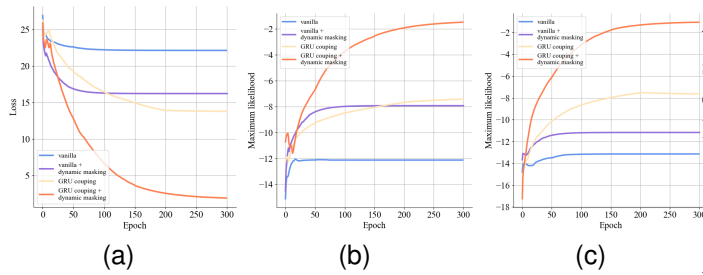


Fig. 11. The loss, energy distribution maximum likelihood, and proposal distribution maximum likelihood in model training

Fig.11 illustrates that the incorporation of the mask mechanism (purple curve) or GRU coupling (yellow curve) into the original network (blue curve) leads to significantly increased maximum likelihood values. However, the introduction of GRU coupling, which necessitates GRU cell embedding, introduces more network parameters, resulting in a slower convergence compared to the original network enhanced with a masking mechanism. The proposed method (orange curve) shows the highest maximum likelihood values, indicating that it can estimate the conditional probability distribution more accurately, and thus obtain more accurate Shapley value estimation results.

## VI. CONCLUSION

This paper proposes a deep learning interpretation framework based on Shapley value and applies it to the field of predictive modeling to explain the contribution of each variable to the predicted results. To enhance the accuracy of Shapley value estimation, this paper introduces a GRU coupled energy-based model to approximate conditional density under arbitrary inputs subsets and use this conditional density to calculate Shapley value. In addition, a dynamic masking scheme is also proposed to improve the model performance. The theoretical analysis on the estimation error bound shows the high accuracy of the proposed method. The proposed method is applied to a medical case and an industrial case, these cases prove that the proposed method is more accurate than the existing methods.

## APPENDIX

In this appendix, the upper error bound of KernelSHAP and variational autoencoder are analyzed, we first show the error bound of KernelSHAP, and then the error bound of the variational autoencoder.

### A. Error Bound of KernelSHAP

KernelSHAP believes that the calculation of the Shapley value can be regarded as an additive model, that is, the contribution function  $v(S)$  of the variable set  $S$  can be approximated by the sum of the variable weights within  $S$ ,

$$v(S) \approx \beta_0 + \sum_{i \in S} \beta_i \quad (A1)$$

where  $\beta_0$  is the mean of  $v(S)$ ,  $\beta_i$  is the weight scalar of the  $i$ -th variable. By designing a linear regression model and solving it using the weighted least square method, the weight of each variable can be obtained. The optimization formula of KernelSHAP is as follows.

$$\min_{\beta_0, \dots, \beta_D} \sum_{S \in D} \psi(S) \left( \beta_0 + \sum_{i \in S} \beta_i - v(S) \right)^2 \quad (A2)$$

where  $\boldsymbol{\beta} = [\beta_0, \dots, \beta_D]^T \in \mathbb{R}^{|D|+1}$  is the weight of each variable,  $\psi = \frac{|S|!(|D|-|S|-1)!}{|D|!}$  is called the Shapley kernel. To solve the above optimization problem, Covert *et al.* [12] introduced an binary vector  $\mathbf{b} \in \mathbb{R}^{|D|+1}$ ,  $b_i = 1$  indicates the  $i$ -th variable is in the subset  $S$ , and otherwise  $b_i = 0$ . Thus, Eq.(A2) can be rewritten as follows.

$$\min_{\boldsymbol{\beta}} \sum_{S \in D} \psi(S) (\mathbf{b}^T \boldsymbol{\beta} - v(S))^2 \quad (A3)$$

The matrix form of Eq.(A3) is as follows.

$$\min_{\boldsymbol{\beta}} \frac{1}{K} (\mathbf{B}^T \boldsymbol{\beta} - \mathbf{v})^T \boldsymbol{\psi} (\mathbf{B}^T \boldsymbol{\beta} - \mathbf{v}) \quad (A4)$$

where  $K$  is the number of sampling times,  $\mathbf{B} \in \mathbb{R}^{(|D|+1) \times K}$  is a binary matrix indicating which variables are in  $S$ ,  $\boldsymbol{\psi} \in \mathbb{R}^{K \times K}$  is a diagonal matrix with Shapley kernel in its diagonal,  $\mathbf{v} \in \mathbb{R}^{K \times 1}$  is the contribution function vector of different samples.

Eq.(A4) can be solved by weighted least square method to obtain the estimation  $\hat{\boldsymbol{\beta}}$ , by taking the first-order derivative of  $\boldsymbol{\beta}$  in Eq.(A4) and setting it to zero, the derivation of weighted least square is given by,

$$\frac{1}{K} (\mathbf{B} \boldsymbol{\psi} \mathbf{B}^T \boldsymbol{\beta} - \mathbf{B}^T \boldsymbol{\psi} \mathbf{v}) = 0 \quad (A5)$$

For the details of KernelSHAP, interested readers can refer to Refs [11], [12].

Let  $\hat{\boldsymbol{\Sigma}} = \frac{1}{K} \mathbf{B} \boldsymbol{\psi} \mathbf{B}^T$  and  $\hat{\boldsymbol{\Gamma}} = \frac{1}{K} \mathbf{B}^T \boldsymbol{\psi} \mathbf{v}$ ,  $\mathbb{E}[\hat{\boldsymbol{\Sigma}}] = \boldsymbol{\Sigma}^*$  and  $\mathbb{E}[\hat{\boldsymbol{\Gamma}}] = \boldsymbol{\Gamma}^*$ . Assuming that  $\hat{\boldsymbol{\Sigma}}$  and  $\boldsymbol{\Sigma}^*$  is invertible, we have  $\hat{\boldsymbol{\beta}} = \hat{\boldsymbol{\Sigma}}^{-1} \hat{\boldsymbol{\Gamma}}$ ,  $\boldsymbol{\beta}^* = \mathbb{E}[\hat{\boldsymbol{\Sigma}}^{-1} \hat{\boldsymbol{\Gamma}}]$ . The error bound of KernelSHAP can be described as the mean absolute deviation between the estimated contribution function  $\hat{v}(S)$  and the true contribution function  $v(S)$ , this error bound is also related to the  $\hat{\boldsymbol{\beta}}$  and  $\boldsymbol{\beta}^*$  as follows.

$$\mathbb{E}[|\hat{v}(S) - v(S)|] = \mathbb{E} \left[ \|\hat{\boldsymbol{\beta}} - \boldsymbol{\beta}^*\| \right] \quad (A6)$$

The decomposition of Eq.(A6) is given by,

$$\begin{aligned} & \mathbb{E}[\|\hat{v}(S) - v(S)\|] \\ &= \mathbb{E}\left[\|\hat{\beta} - \beta^*\|\right] = \mathbb{E}[\|\hat{\Sigma}^{-1}\hat{\Gamma} - \mathbb{E}[\hat{\Sigma}^{-1}\hat{\Gamma}]\|] \\ &= \mathbb{E}[\|\hat{\Sigma}^{-1}\hat{\Gamma} - \mathbb{E}[\hat{\Sigma}^{-1}]\mathbb{E}[\hat{\Gamma}] - \text{cov}(\hat{\Sigma}^{-1}, \hat{\Gamma})\|] \\ &= \mathbb{E}[\|\hat{\Sigma}^{-1}\hat{\Gamma} - \Sigma^{*-1}\Gamma^* - \text{cov}(\hat{\Sigma}^{-1}, \hat{\Gamma})\|] \end{aligned} \quad (\text{A7})$$

where  $\|\cdot\|$  is the  $L_2$  norm and  $\text{cov}(\cdot, \cdot)$  is the covariance. Next we introduce three corollaries and show that  $\text{cov}(\hat{\Sigma}^{-1}, \hat{\Gamma}) \rightarrow 0$  in some specific cases.

**Corollary A1.** (Concentration of  $\hat{\Sigma}$ ) For all  $\varepsilon_2 > 0$ , we have,

$$\mathbb{P}(\|\hat{\Sigma} - \Sigma^*\| \geq \varepsilon_2) \leq 2(|D|+1)^2 \exp(-2K\varepsilon_2^2) \quad (\text{A8})$$

*Proof.* Noting that the elements in  $\mathbf{B}$  are 0 or 1 and the elements in  $\mathbf{y}$  is bounded with  $[0, 1]$ . Thus the element in  $\hat{\Sigma}$  and  $\Sigma^*$  also bounded with  $[0, 1]$ . According to Hoeffding's inequality, each element in  $\hat{\Sigma}$  is bounded with their expectation values, that is, for all  $\varepsilon > 0$

$$\begin{cases} \mathbb{P}(|\frac{1}{K} \sum_{k=1}^K (\hat{\Sigma}_{ii} - \mathbb{E}[\hat{\Sigma}_{ii}])| \geq \varepsilon_2) \leq 2 \exp(-2K\varepsilon_2^2) \\ \mathbb{P}(|\frac{1}{K} \sum_{k=1}^K (\hat{\Sigma}_{ij} - \mathbb{E}[\hat{\Sigma}_{ij}])| \geq \varepsilon_2) \leq 2 \exp(-2K\varepsilon_2^2) \end{cases} \quad (\text{A9})$$

where,  $\mathbb{E}[\hat{\Sigma}_{ii}] = \frac{1}{2}$  and  $\mathbb{E}[\hat{\Sigma}_{ij}] = \alpha$ , so

$$\begin{cases} \mathbb{P}(|\frac{1}{K} \sum_{k=1}^K (\hat{\Sigma}_{ii} - \frac{1}{2})| \geq \varepsilon_2) \leq 2 \exp(-2K\varepsilon_2^2) \\ \mathbb{P}(|\frac{1}{K} \sum_{k=1}^K (\hat{\Sigma}_{ij} - \alpha)| \geq \varepsilon_2) \leq 2 \exp(-2K\varepsilon_2^2) \end{cases} \quad (\text{A10})$$

By using Boole's inequality [36], Eq.(A8) can be obtained.  $\square$

The concentration of  $\hat{\Gamma}$  can be obtained in the same.

**Corollary A2.** (Concentration of  $\hat{\Gamma}$ ) For all  $\varepsilon_2 > 0$ , we have,

$$\mathbb{P}(\|\hat{\Gamma} - \Gamma^*\| \geq \varepsilon_2) \leq 2(|D|+1) \exp(-2K\varepsilon_2^2) \quad (\text{A11})$$

*Proof.* According to Assumption 4, the contribution value of any subset  $S$  is bounded within  $[0, 1]$ , that is  $v(S) \in [0, 1]$ . Then  $\mathbf{v}$  is also bounded within  $[0, 1]$ , which indicates  $\Gamma^* \in [0, 1]$ , by using Hoeffding's inequality, each element in  $\hat{\Gamma}$  is bounded with their expectation values, that is, for all  $\varepsilon > 0$

$$\mathbb{P}\left(\left|\frac{1}{K} \sum_{k=1}^K (\hat{\Gamma}_i - \mathbb{E}[\hat{\Gamma}_i])\right| \geq \varepsilon_2\right) \leq 2 \exp(-2K\varepsilon_2^2) \quad (\text{A12})$$

By using Boole's inequality [36], the concentration of  $\hat{\Gamma}$  can be obtained.  $\square$

**Corollary A3.** For the fixed input dimension  $|D|$ , when sampling number  $K$  goes to positive infinity, there exists a small positive number  $\varepsilon$  that,

$$\mathbb{P}\left(\|\text{cov}(\hat{\Sigma}^{-1}, \hat{\Gamma})\| \geq \varepsilon\right) \leq 2((|D|+1)^2 + (|D|+1)) \exp(-2K\varepsilon_2^2) \quad (\text{A13})$$

where  $\varepsilon \in [\sqrt{\frac{1}{2K} \log(2((|D|+1)^2 + (|D|+1)))}, +\infty)$ , and for any fixed input dimension  $|D|$ , when  $K$  goes to positive infinity, with the probability greater than  $1 - 2((|D|+1)^2 + (|D|+1)) \exp(-2K\varepsilon_2^2)$ , we have,

$$\|\text{cov}(\hat{\Sigma}^{-1}, \hat{\Gamma})\| \leq \varepsilon_2^2 \quad (\text{A14})$$

*Proof.* According to Corollaries A1, A2 and Boole's inequality, Eq.(A13) can be obtained. Since the probabil-

ity  $\mathbb{P}\left(\|\text{cov}(\hat{\Sigma}^{-1}, \hat{\Gamma})\| \geq \varepsilon_2\right) \in [0, 1]$ , the range of  $\varepsilon_2$  is  $[\sqrt{\frac{1}{2K} \log(2((|D|+1)^2 + (|D|+1)))}, +\infty)$ .

The proof of Eq.(A14) is as follows, for fixed  $|D|$  and when  $K$  goes to positive infinity, under the probability greater than  $1 - 2((|D|+1)^2 + (|D|+1)) \exp(-2K\varepsilon_2^2)$ ,

$$\begin{aligned} \|\text{cov}(\hat{\Sigma}^{-1}, \hat{\Gamma})\| &= \left\| \mathbb{E}\left[\left(\hat{\Sigma}^{-1} - \mathbb{E}[\hat{\Sigma}^{-1}]\right)\left(\hat{\Gamma} - \mathbb{E}[\hat{\Gamma}]\right)\right] \right\| \\ &= \left\| \mathbb{E}\left[\left(\hat{\Sigma}^{-1} - \Sigma^{*-1}\right)\left(\hat{\Gamma} - \Gamma^*\right)\right] \right\| \leq \varepsilon_2^2 \end{aligned} \quad (\text{A15})$$

It should be notice that when  $K$  goes to positive infinity, the probability  $1 - 2((|D|+1)^2 + (|D|+1)) \exp(-2K\varepsilon_2^2)$  close to 1, which means  $\|\text{cov}(\hat{\Sigma}^{-1}, \hat{\Gamma})\| \leq \varepsilon_2^2$  holds true under almost any conditions.  $\square$

Thus, Eq.(A7) can be rewritten as follows,

$$\begin{aligned} & \mathbb{E}[\|\hat{v}(S) - v(S)\|] \\ & \leq \mathbb{E}[\|\hat{\Sigma}^{-1}\hat{\Gamma} - \Sigma^{*-1}\Gamma^*\|] + \mathbb{E}[\|\cdot - \text{cov}(\hat{\Sigma}^{-1}, \hat{\Gamma})\|] \\ & \leq \mathbb{E}[\|\hat{\Sigma}^{-1}\hat{\Gamma} - \Gamma^*\|] + \mathbb{E}[\|\hat{\Sigma}^{-1} - \Sigma^{*-1}\Gamma^*\|] + \varepsilon_2^2 \\ & \leq \mathbb{E}[\|\hat{\Sigma}^{-1}\| \cdot \|\hat{\Gamma} - \Gamma^*\|] + \mathbb{E}[\|\hat{\Sigma}^{-1} - \Sigma^{*-1}\| \cdot \|\Gamma^*\|] + \varepsilon_2^2 \\ & = \mathbb{E}[\|\hat{\Sigma}^{-1}\hat{\Gamma} - \Gamma^*\|] + \mathbb{E}[\|\Sigma^{*-1}(\hat{\Sigma} - \Sigma^*)\hat{\Sigma}^{-1}\| \cdot \|\Gamma^*\|] + \varepsilon_2^2 \\ & \leq \mathbb{E}[\|\hat{\Sigma}^{-1}\| \cdot \|\hat{\Gamma} - \Gamma^*\|] + \mathbb{E}[\|\Sigma^{*-1}\| \cdot \|\hat{\Sigma} - \Sigma^*\| \cdot \|\hat{\Sigma}^{-1}\| \cdot \|\Gamma^*\|] + \varepsilon_2^2 \end{aligned} \quad (\text{A16})$$

By calculating the upper bounds of the decomposed elements in Eq.(eq-a-24-3) separately and merging them, the upper bound of  $\mathbb{E}[\|\hat{v}(S) - v(S)\|]$  can be obtained. Notice that Ref. [37] gives the theoretical analysis of LIME, we follow their contribution and derive the error bound of KernelSHAP. Here, the explicit expressions of  $\Sigma^*$  and its inverse form  $\Sigma^{*-1}$  are first into consideration. According to Ref. [12],  $\Sigma^*$  has the following form,

$$\Sigma^* = \begin{bmatrix} \frac{1}{2} & \alpha & \cdots & \alpha \\ \alpha & \frac{1}{2} & \cdots & \alpha \\ \vdots & \vdots & \ddots & \vdots \\ \alpha & \alpha & \cdots & \frac{1}{2} \end{bmatrix} \quad (\text{A17})$$

that is, the diagonal of  $\Sigma^*$  is  $\frac{1}{2}$ , and the off-diagonal entries are  $\alpha$ , where

$$\alpha = \frac{1}{|D|(|D|+1)} \frac{\sum_{i=2}^{|D|} \frac{i-1}{|D|+1-i}}{\sum_{i=1}^{|D|} \frac{1}{i(|D|+1-i)}} \quad (\text{A18})$$

**Lemma A1.** Assuming  $\Sigma^*$  is invertible, the inverse of  $\Sigma^*$ ,  $\Sigma^{*-1}$ , has the following expression,

$$\Sigma^{*-1} = \begin{bmatrix} \frac{1}{\frac{1}{2}-\alpha} & \frac{\alpha}{(\alpha-\frac{1}{2})(K\alpha-\alpha+\frac{1}{2})} & \cdots & \frac{\alpha}{(\alpha-\frac{1}{2})(K\alpha-\alpha+\frac{1}{2})} \\ \frac{\alpha}{(\alpha-\frac{1}{2})(K\alpha-\alpha+\frac{1}{2})} & \frac{1}{\frac{1}{2}-\alpha} & \cdots & \frac{\alpha}{(\alpha-\frac{1}{2})(K\alpha-\alpha+\frac{1}{2})} \\ \vdots & \vdots & \ddots & \vdots \\ \frac{\alpha}{(\alpha-\frac{1}{2})(K\alpha-\alpha+\frac{1}{2})} & \frac{\alpha}{(\alpha-\frac{1}{2})(K\alpha-\alpha+\frac{1}{2})} & \cdots & \frac{1}{\frac{1}{2}-\alpha} \end{bmatrix} \quad (\text{A19})$$

*Proof.* According to Eq.(A17),  $\Sigma^*$  can be decomposed as follows,

$$\Sigma^* = \left(\frac{1}{2} - \alpha\right)\mathbf{I} + \alpha\mathbf{J} \quad (\text{A20})$$

where  $\mathbf{I} \in \mathbb{R}^{(|D|+1) \times (|D|+1)}$  is a identity matrix and  $\mathbf{J} \in \mathbb{R}^{(|D|+1) \times (|D|+1)}$  is a matrix with all ones. Let  $\Sigma^{*-1} = \kappa\mathbf{I} + \omega\mathbf{J}$ ,  $\kappa$  and  $\omega$  are need to be determined, we have,

$$\left( \left( \frac{1}{2} - \alpha \right) \mathbf{I} + \alpha \mathbf{J} \right) (\kappa \mathbf{I} + \omega \mathbf{J}) = \mathbf{I} \quad (\text{A21})$$

By sorting out the above formula,

$$\left( \frac{1}{2} - \alpha \right) \kappa \mathbf{I} + \left[ \left( \frac{1}{2} - \alpha + K\alpha \right) \omega + \kappa \alpha \right] \mathbf{J} = \mathbf{I} \quad (\text{A22})$$

Thus, we can get,

$$\begin{cases} \left( \frac{1}{2} - \alpha \right) \kappa = 1 \\ \left( \frac{1}{2} - \alpha + K\alpha \right) \omega + \kappa \alpha = 0 \end{cases} \quad (\text{A23})$$

By solving Eq.(A23), we have,

$$\kappa = \frac{1}{\frac{1}{2} - \alpha}, \quad \omega = \frac{\alpha}{(\alpha - \frac{1}{2})(K\alpha - \alpha + \frac{1}{2})} \quad (\text{A24})$$

and

$$\Sigma^{*-1} = \frac{1}{\frac{1}{2} - \alpha} \mathbf{I} + \frac{\alpha}{(\alpha - \frac{1}{2})(K\alpha - \alpha + \frac{1}{2})} \mathbf{J} \quad (\text{A25})$$

□

**Proposition A1.** (The upper bound of  $\|\Sigma^{*-1}\|$ ) The  $L_2$  norm of  $\Sigma^{*-1}$  is upper bounded with,

$$\|\Sigma^{*-1}\| \leq \sqrt{\frac{|D|+1}{(\frac{1}{2}-\alpha)^2} + \frac{(|D|+1)|D|\alpha^2}{((\alpha-\frac{1}{2})(K\alpha-\alpha+\frac{1}{2}))^2}} \quad (\text{A26})$$

*Proof.* The square  $L_2$  norm of  $\Sigma^{*-1}$  is upper bounded by its Frobenius norm, that is,

$$\|\Sigma^{*-1}\|^2 \leq \|\Sigma^{*-1}\|_F^2 = \frac{|D|+1}{(\frac{1}{2}-\alpha)^2} + \frac{(|D|+1)|D|\alpha^2}{((\alpha-\frac{1}{2})(K\alpha-\alpha+\frac{1}{2}))^2} \quad (\text{A27})$$

By taking the root square on both sides of Eq.(A26), we can get Eq.(A27). □

Similarly, the upper bound of  $\|\Gamma^*\|$  can be obtained in the same way.

**Proposition A2.** (Upper bound of  $\|\Gamma^*\|$ ) The  $L_2$  norm of  $\Gamma^*$  is upper bounded with,

$$\|\Gamma^*\| \leq \sqrt{|D|+1} \quad (\text{A28})$$

*Proof.* The square  $L_2$  norm of  $\Gamma^*$  is as follows.

$$\|\Gamma^*\|^2 = \|\mathbf{B}\psi\mathbf{v}\|^2 \quad (\text{A29})$$

Since each element in  $\Gamma^*$  is bounded within  $[0, 1]$ , the square  $L_2$  norm of  $\Gamma^*$  is smaller then its dimension, that is,  $\|\Gamma^*\|^2 \leq |D|+1$ . □

**Proposition A3.** (Upper bound of  $\hat{\Sigma}^{-1}$ ) For all  $\varepsilon \in (0, \frac{1}{\|\Sigma^{*-1}\|_F})$ , with the probability greater than  $1 - 2(|D|+1)^2 \exp(-2K\varepsilon^2)$ ,

$$\|\hat{\Sigma}^{-1}\| \leq \frac{\|\Sigma^{*-1}\|_F}{1 - \varepsilon \|\Sigma^{*-1}\|_F} \leq \|\Sigma^{*-1}\|_F \quad (\text{A30})$$

*Proof.* According to Lemma A1, we have  $\lambda_{\max}(\Sigma^{*-1}) \leq \|\Sigma^{*-1}\|_F$ . Thus, we have,

$$\lambda_{\min}(\Sigma^*) \geq \frac{1}{\|\Sigma^{*-1}\|_F} \quad (\text{A31})$$

Particularly,  $\hat{\Sigma}$  is concentrated on  $\Sigma^*$ , by using Weyl' inequality [38],

$$|\lambda_{\min}(\hat{\Sigma}) - \lambda_{\min}(\Sigma^*)| \leq \|\hat{\Sigma} - \Sigma^*\| \leq \varepsilon \quad (\text{A32})$$

and,

$$\lambda_{\min}(\hat{\Sigma}) \geq \lambda_{\min}(\Sigma^*) - \varepsilon \geq \frac{1}{\|\Sigma^{*-1}\|_F} - \varepsilon \quad (\text{A33})$$

which can be deduced to

$$\|\hat{\Sigma}^{-1}\| \leq \frac{\|\Sigma^{*-1}\|_F}{1 - \varepsilon \|\Sigma^{*-1}\|_F} \quad (\text{A34})$$

Since  $\varepsilon > 0$  and  $\|\Sigma^{*-1}\|_F > 0$ , when  $\varepsilon$  goes to zero, we have  $\|\hat{\Sigma}^{-1}\| \leq \|\Sigma^{*-1}\|_F$ . □

Therefore, for fixed feature dimension  $|D|$  and when sampling number  $K$  goes to zeros, the final result of  $\mathbb{E}[\|\hat{v}(S) - v(S)\|]$  with the probability greater than  $1 - 2((|D|+1)^2 + (|D|+1)) \exp(-2K\varepsilon_2^2)$  is as follows.

$$\begin{aligned} & \mathbb{E}[\|\hat{v}(S) - v(S)\|] \\ & \leq \mathbb{E}[\|\hat{\Sigma}^{-1}\| \cdot \|\hat{\Gamma} - \Gamma^*\|] + \mathbb{E}[\|\Sigma^{*-1}\| \cdot \|\hat{\Sigma} - \Sigma^*\| \cdot \|\hat{\Sigma}^{-1}\| \cdot \|\Gamma^*\|] + \varepsilon_2^2 \\ & \leq \|\Sigma^{*-1}\|_F \cdot \int_0^{+\infty} 2(|D|+1) \exp(-2K\varepsilon_2^2) d\varepsilon_2 + \varepsilon_2^2 \\ & \quad + \|\Sigma^{*-1}\|_F \cdot \int_0^{+\infty} 2(|D|+1)^2 \exp(-2K\varepsilon_2^2) d\varepsilon_2 \cdot \|\Sigma^{*-1}\|_F \cdot \sqrt{|D|+1} \\ & = 2(|D|+1) \frac{\sqrt{\pi}}{\sqrt{2K}} \|\Sigma^{*-1}\|_F + 2(|D|+1)^{\frac{5}{2}} \frac{\sqrt{\pi}}{\sqrt{2K}} \|\Sigma^{*-1}\|_F^2 + \varepsilon_2^2 \end{aligned} \quad (\text{A35})$$

It can be seen from Eq.(A35) that as the data dimension  $|D|$  increases, the error estimated by KernelSHAP will increase. On the other hand, the estimation error will decrease as the number of samples  $K$  increases.

## B. Error Bound of Variational autoencoder

Variational autoencoder (VAE) is a typical generative model, which uses a latent variable model to give a probabilistic representation of the unknown data distribution  $p(\mathbf{x})$ . The basic idea of the variational autoencoder is to generate the observed variable  $\mathbf{x}$  through a simple distributed latent variable  $\mathbf{z}$ . Specifically, VAE first models the joint distribution,

$$p(\mathbf{x}, \mathbf{z}) = p(\mathbf{z})p_{\theta}(\mathbf{x}|\mathbf{z}) \quad (\text{B1})$$

where the conditional distribution  $p_{\theta}(\mathbf{x}|\mathbf{z})$  is called an encoder, which is modeled by a deep neural network with parameter  $\theta$ ,  $\mathbf{z}$  is the latent variable with simple distribution, such as standard normal distribution. By marginalizing the latent variable, the data distribution can be approximated.

$$p(\mathbf{x}) = \int p(\mathbf{x}, \mathbf{z}) d\mathbf{z} \quad (\text{B2})$$

This latent variable model helps to get  $p(\mathbf{x})$  easily. However, the calculation of the posterior distribution  $p_\theta(\mathbf{z}|\mathbf{x})$  during training becomes intractable. To address this challenge, VAE constructs a distribution  $q_\tau(\mathbf{z}|\mathbf{x})$  to approximate  $p_\theta(\mathbf{z}|\mathbf{x})$ , which is called the decoder parameterized with  $\tau$ . The data log-likelihood of VAE can be expressed as follows.

$$\begin{aligned}
\log p_\theta(\mathbf{x}) &= \log p_\theta(\mathbf{x}) \int q_\tau(\mathbf{z}|\mathbf{x}) d\mathbf{z} \\
&= \int q_\tau(\mathbf{z}|\mathbf{x}) \log p_\theta(\mathbf{x}) d\mathbf{z} \\
&= \mathbb{E}_{q_\tau(\mathbf{z}|\mathbf{x})} \log p_\theta(\mathbf{x}) \\
&= \mathbb{E}_{q_\tau(\mathbf{z}|\mathbf{x})} \log \frac{p_\theta(\mathbf{x}, \mathbf{z})}{p_\theta(\mathbf{z}|\mathbf{x})} \\
&= \mathbb{E}_{q_\tau(\mathbf{z}|\mathbf{x})} \log \frac{p_\theta(\mathbf{x}, \mathbf{z}) q_\tau(\mathbf{z}|\mathbf{x})}{p_\theta(\mathbf{z}|\mathbf{x}) q_\tau(\mathbf{z}|\mathbf{x})} \\
&= \mathbb{E}_{q_\tau(\mathbf{z}|\mathbf{x})} \log \frac{p_\theta(\mathbf{x}, \mathbf{z})}{q_\tau(\mathbf{z}|\mathbf{x})} + \mathbb{E}_{q_\tau(\mathbf{z}|\mathbf{x})} \log \frac{q_\tau(\mathbf{z}|\mathbf{x})}{p_\theta(\mathbf{z}|\mathbf{x})} \\
&= \mathbb{E}_{q_\tau(\mathbf{z}|\mathbf{x})} \log \frac{p_\theta(\mathbf{x}, \mathbf{z})}{q_\tau(\mathbf{z}|\mathbf{x})} + D_{KL}(q_\tau(\mathbf{z}|\mathbf{x}) || p_\theta(\mathbf{z}|\mathbf{x})) \tag{B3}
\end{aligned}$$

where  $\mathbb{E}_{q_\tau(\mathbf{z}|\mathbf{x})} \log \frac{p_\theta(\mathbf{x}, \mathbf{z})}{q_\tau(\mathbf{z}|\mathbf{x})}$  is called evidence lower bound (ELBO) and  $D_{KL}(\cdot || \cdot)$  is Kullback-Leibler (KL) divergence. ELBO is the object function needs to be optimized, by maximizing ELBO via gradient descent, the fine-trained VAE can be obtained.  $D_{KL}(q_\tau(\mathbf{z}|\mathbf{x}) || p_\theta(\mathbf{z}|\mathbf{x}))$  shows the gap between log-likelihood and ELBO, which is exactly the mismatch between VAE encoder and the posterior [39].

Ref. [17] introduces a Shapley value approximation approach based on VAE. The contribution function of Shapley value is sampled from the conditional probability  $p_\theta(\mathbf{x}_{\bar{S}}|\mathbf{x}_S)$  generated by VAE and the sampling method is just like the method proposed in this article. The log-likelihood introduced in Ref. [17] is as follows.

$$\begin{aligned}
\log p_\theta(\mathbf{x}_{\bar{S}}|\mathbf{x}_S) &= \mathbb{E}_{q_\tau(\mathbf{z}|\mathbf{x}_{\bar{S}}, \mathbf{x}_S)} \left[ \log \frac{p_\theta(\mathbf{x}_{\bar{S}}, \mathbf{z}|\mathbf{x}_S)}{q_\tau(\mathbf{z}|\mathbf{x}_{\bar{S}}, \mathbf{x}_S)} \right] + \mathbb{E}_{q_\tau(\mathbf{z}|\mathbf{x}_{\bar{S}}, \mathbf{x}_S)} \left[ \log \frac{q_\tau(\mathbf{z}|\mathbf{x}_{\bar{S}}, \mathbf{x}_S)}{p_\theta(\mathbf{z}|\mathbf{x}_{\bar{S}}, \mathbf{x}_S)} \right] \\
&= \mathbb{E}_{q_\tau(\mathbf{z}|\mathbf{x}_{\bar{S}}, \mathbf{x}_S)} \left[ \log \frac{p_\theta(\mathbf{x}_{\bar{S}}, \mathbf{z}|\mathbf{x}_S)}{q_\tau(\mathbf{z}|\mathbf{x}_{\bar{S}}, \mathbf{x}_S)} \right] + D_{KL}(q_\tau(\mathbf{z}|\mathbf{x}_{\bar{S}}, \mathbf{x}_S) || p_\theta(\mathbf{z}|\mathbf{x}_{\bar{S}}, \mathbf{x}_S)) \\
&\geq \mathbb{E}_{q_\tau(\mathbf{z}|\mathbf{x}_{\bar{S}}, \mathbf{x}_S)} \left[ \log \frac{p_\theta(\mathbf{x}_{\bar{S}}, \mathbf{z}|\mathbf{x}_S)}{q_\tau(\mathbf{z}|\mathbf{x}_{\bar{S}}, \mathbf{x}_S)} \right] \tag{B4}
\end{aligned}$$

This VAE-based Shapley value estimation method trains the parameters in the VAE by maximizing the first term in Eq.(B4), and then samples from the generated conditional distribution  $p_\theta(\mathbf{x}_{\bar{S}}|\mathbf{x}_S)$  to calculate the contribution function  $v$  in the Shapley value and the Shapley values of each input.

However, a problem arises here, that the generated conditional distribution  $p_\theta(\mathbf{x}_{\bar{S}}|\mathbf{x}_S)$  converges to the true conditional distribution  $p_{data}(\mathbf{x}_{\bar{S}}|\mathbf{x}_S)$  if and only if  $D_{KL}(q_\tau(\mathbf{z}|\mathbf{x}_{\bar{S}}, \mathbf{x}_S) || p_\theta(\mathbf{z}|\mathbf{x}_{\bar{S}}, \mathbf{x}_S))$  goes to zeros. Unfortunately, it's not explicit to ensure this happens, since  $q_\tau(\mathbf{z}|\mathbf{x}_{\bar{S}}, \mathbf{x}_S)$  is modeled as exponential families, i.e. multivariate Gaussian distribution, the posterior distribution  $p_\theta(\mathbf{z}|\mathbf{x})$  is not always possible to use the exponential families to approximate. Thus, for an unknown data distribution  $p(\mathbf{x})$ ,  $D_{KL}(q_\tau(\mathbf{z}|\mathbf{x}_{\bar{S}}, \mathbf{x}_S) || p_\theta(\mathbf{z}|\mathbf{x}_{\bar{S}}, \mathbf{x}_S))$  is hardly going to zeros, which indicates that there is a inference gap between the true distribution and the generated distribution.

According to Ref. [40], the inference gap of VAE is decomposed into two components, the approximation gap  $\log p_{data}(\mathbf{x}) - \log p_{\theta^*}(\mathbf{x})$  and the amortization gap  $\log p_{\theta^*}(\mathbf{x}) - \log p_\theta(\mathbf{x})$ , where  $\theta^* \in \operatorname{argmin}_\theta \log p_\theta(\mathbf{x})$ . Since the analysis of the model error bound in this paper assumes that the model can achieve theoretical optimal performance after a large number of iterative training, the amortized error of VAE here is negligible. We focus on the approximation gap, followed by the above discussion, we have,

$$\begin{aligned}
&\log p_{data}(\mathbf{x}_{\bar{S}}|\mathbf{x}_S) - \log p_{\theta^*}(\mathbf{x}_{\bar{S}}|\mathbf{x}_S) \\
&= D_{KL}(q_\tau(\mathbf{z}|\mathbf{x}_{\bar{S}}, \mathbf{x}_S) || p_\theta(\mathbf{z}|\mathbf{x}_{\bar{S}}, \mathbf{x}_S)) \tag{B5}
\end{aligned}$$

Eq.(B5) shows the difference between the log-likelihood of  $\log p_{data}(\mathbf{x})$  and  $\log p_{\theta^*}(\mathbf{x})$ , this difference also leads to the probability density difference,

$$\left| \frac{p_{\theta^*}(\mathbf{x}_{\bar{S}}|\mathbf{x}_S = \mathbf{x}_S^*))}{p_{data}(\mathbf{x}_{\bar{S}}|\mathbf{x}_S = \mathbf{x}_S^*))} - 1 \right| \leq \delta \tag{B6}$$

where  $\delta$  is the difference of the probability density between  $p_{data}$  and  $p_{\theta^*}$ . It should be noted that  $\delta$  is positive related to  $D_{KL}(q_\tau(\mathbf{z}|\mathbf{x}) || p_\theta(\mathbf{z}|\mathbf{x}))$ . Let  $\Delta = |\hat{v}(S) - v(S)|$  and  $\mathbb{E}[\Delta]$  be the expectation of  $\Delta$ . The upper bound of the VAE-based approach is given as follows.

Similar to Assumption 1, assuming that the parameters of the estimated conditional density  $p_\theta(\mathbf{x}_{\bar{S}}|\mathbf{x}_S = \mathbf{x}_S^*)$  are unbiased estimates of the parameters of the optimal estimated density  $p_{\theta^*}(\mathbf{x}_{\bar{S}}|\mathbf{x}_S = \mathbf{x}_S^*)$ , and for a small positive  $\varepsilon_1$ , the probability density ratio is as follows.

$$\left| \frac{p_\theta(\mathbf{x}_{\bar{S}}|\mathbf{x}_S = \mathbf{x}_S^*)}{p_{\theta^*}(\mathbf{x}_{\bar{S}}|\mathbf{x}_S = \mathbf{x}_S^*)} - 1 \right| \leq \varepsilon_1 \tag{B7}$$

Then we begin the analysis of VAEAC method. Firstly,  $\mathbb{E}[\Delta]$  of VAE-based approach can be derived as follows.

$$\begin{aligned}
&\mathbb{E}[|\hat{v}(S) - v(S)|] \\
&= \mathbb{E} \left[ \left| \frac{1}{k} \sum_{k=1}^K f(\mathbf{x}_{\bar{S}}^{(k)}, \mathbf{x}_S^*) - \mathbb{E}_{p_{data}(\mathbf{x}_{\bar{S}}|\mathbf{x}_S = \mathbf{x}_S^*)} [f(\mathbf{x}_{\bar{S}}^*, \mathbf{x}_S^*)] \right| \right] \\
&= \mathbb{E} \left[ \left| \frac{1}{k} \sum_{k=1}^K f(\mathbf{x}_{\bar{S}}^{(k)}, \mathbf{x}_S^*) - \mathbb{E}_{p_\theta(\mathbf{x}_{\bar{S}}|\mathbf{x}_S = \mathbf{x}_S^*)} [f(\mathbf{x}_{\bar{S}}, \mathbf{x}_S^*)] \right. \right. \\
&\quad \left. \left. + \mathbb{E}_{p_\theta(\mathbf{x}_{\bar{S}}|\mathbf{x}_S = \mathbf{x}_S^*)} [f(\mathbf{x}_{\bar{S}}, \mathbf{x}_S^*)] - \mathbb{E}_{p_{\theta^*}(\mathbf{x}_{\bar{S}}|\mathbf{x}_S = \mathbf{x}_S^*)} [f(\mathbf{x}_{\bar{S}}, \mathbf{x}_S^*)] \right. \right. \\
&\quad \left. \left. + \mathbb{E}_{p_{\theta^*}(\mathbf{x}_{\bar{S}}|\mathbf{x}_S = \mathbf{x}_S^*)} [f(\mathbf{x}_{\bar{S}}, \mathbf{x}_S^*)] - \mathbb{E}_{p_{data}(\mathbf{x}_{\bar{S}}|\mathbf{x}_S = \mathbf{x}_S^*)} [f(\mathbf{x}_{\bar{S}}^*, \mathbf{x}_S^*)] \right| \right] \\
&\leq \mathbb{E} \left[ \left| \frac{1}{k} \sum_{k=1}^K f(\mathbf{x}_{\bar{S}}^{(k)}, \mathbf{x}_S^*) - \mathbb{E}_{p_\theta(\mathbf{x}_{\bar{S}}|\mathbf{x}_S = \mathbf{x}_S^*)} [f(\mathbf{x}_{\bar{S}}, \mathbf{x}_S^*)] \right| \right] \\
&\quad + \mathbb{E} \left[ \left| \mathbb{E}_{p_\theta(\mathbf{x}_{\bar{S}}|\mathbf{x}_S = \mathbf{x}_S^*)} [f(\mathbf{x}_{\bar{S}}, \mathbf{x}_S^*)] - \mathbb{E}_{p_{\theta^*}(\mathbf{x}_{\bar{S}}|\mathbf{x}_S = \mathbf{x}_S^*)} [f(\mathbf{x}_{\bar{S}}, \mathbf{x}_S^*)] \right| \right] \\
&\quad + \mathbb{E} \left[ \left| \mathbb{E}_{p_{\theta^*}(\mathbf{x}_{\bar{S}}|\mathbf{x}_S = \mathbf{x}_S^*)} [f(\mathbf{x}_{\bar{S}}, \mathbf{x}_S^*)] - \mathbb{E}_{p_{data}(\mathbf{x}_{\bar{S}}|\mathbf{x}_S = \mathbf{x}_S^*)} [f(\mathbf{x}_{\bar{S}}^*, \mathbf{x}_S^*)] \right| \right]
\end{aligned}$$

The first term in the last inequality of Eq.(B8) is called approximation error, and the second is called statistical error. The upper bound of the approximation error is the same as Eq.(33),

$$\mathbb{E} \left[ \left| \frac{1}{k} \sum_{k=1}^K f(\mathbf{x}_{\bar{S}}^{(k)}, \mathbf{x}_S^*) - \mathbb{E}_{p_\theta(\mathbf{x}_{\bar{S}}|\mathbf{x}_S = \mathbf{x}_S^*)} [f(\mathbf{x}_{\bar{S}}, \mathbf{x}_S^*)] \right| \right] \leq \frac{\sqrt{\pi}}{\sqrt{2K}} \tag{B8}$$

The statistical error is related to the amortization gap and

the approximation gap, the error introduced from amortization gap can be described as follows, which is similar to Eq.( 32).

$$\begin{aligned}
& \mathbb{E} \left[ \left| \mathbb{E}_{p_\theta(\mathbf{x}_{\bar{S}}|\mathbf{x}_S=\mathbf{x}_S^*)} [f(\mathbf{x}_{\bar{S}}, \mathbf{x}_S^*)] - \mathbb{E}_{p_{\theta^*}(\mathbf{x}_{\bar{S}}|\mathbf{x}_S=\mathbf{x}_S^*)} [f(\mathbf{x}_{\bar{S}}, \mathbf{x}_S^*)] \right| \right] \\
&= \mathbb{E} \left[ \left| \int f(\mathbf{x}_{\bar{S}}, \mathbf{x}_S^*) p_\theta(\mathbf{x}_{\bar{S}}|\mathbf{x}_S=\mathbf{x}_S^*) d\mathbf{x}_{\bar{S}} - \int f(\mathbf{x}_{\bar{S}}, \mathbf{x}_S^*) p_{\theta^*}(\mathbf{x}_{\bar{S}}|\mathbf{x}_S=\mathbf{x}_S^*) d\mathbf{x}_{\bar{S}} \right| \right] \\
&= \mathbb{E} \left[ \left| \int f(\mathbf{x}_{\bar{S}}, \mathbf{x}_S^*) \frac{p_\theta(\mathbf{x}_{\bar{S}}|\mathbf{x}_S=\mathbf{x}_S^*)}{p_{\theta^*}(\mathbf{x}_{\bar{S}}|\mathbf{x}_S=\mathbf{x}_S^*)} p_{\theta^*}(\mathbf{x}_{\bar{S}}|\mathbf{x}_S=\mathbf{x}_S^*) d\mathbf{x}_{\bar{S}} - \int f(\mathbf{x}_{\bar{S}}, \mathbf{x}_S^*) p_{\theta^*}(\mathbf{x}_{\bar{S}}|\mathbf{x}_S=\mathbf{x}_S^*) d\mathbf{x}_{\bar{S}} \right| \right] \\
&= \mathbb{E} \left[ \left| \mathbb{E}_{p_{\theta^*}(\mathbf{x}_{\bar{S}}|\mathbf{x}_S=\mathbf{x}_S^*)} \left[ \left( f(\mathbf{x}_{\bar{S}}, \mathbf{x}_S^*) \frac{p_\theta(\mathbf{x}_{\bar{S}}|\mathbf{x}_S=\mathbf{x}_S^*)}{p_{\theta^*}(\mathbf{x}_{\bar{S}}|\mathbf{x}_S=\mathbf{x}_S^*)} - f(\mathbf{x}_{\bar{S}}, \mathbf{x}_S^*) \right) \right] \right| \right] \\
&\leq \mathbb{E} \left[ \mathbb{E}_{p_{\theta^*}(\mathbf{x}_{\bar{S}}|\mathbf{x}_S=\mathbf{x}_S^*)} \left[ \left| f(\mathbf{x}_{\bar{S}}, \mathbf{x}_S^*) \frac{p_\theta(\mathbf{x}_{\bar{S}}|\mathbf{x}_S=\mathbf{x}_S^*)}{p_{\theta^*}(\mathbf{x}_{\bar{S}}|\mathbf{x}_S=\mathbf{x}_S^*)} - f(\mathbf{x}_{\bar{S}}, \mathbf{x}_S^*) \right| \right] \right] \\
&= \varepsilon_1
\end{aligned} \tag{B9}$$

The the error introduced from approximation gap can be described as follows,

$$\begin{aligned}
& \mathbb{E} \left[ \left| \mathbb{E}_{p_{\theta^*}(\mathbf{x}_{\bar{S}}|\mathbf{x}_S=\mathbf{x}_S^*)} [f(\mathbf{x}_{\bar{S}}, \mathbf{x}_S^*)] - \mathbb{E}_{p_{data}(\mathbf{x}_{\bar{S}}|\mathbf{x}_S=\mathbf{x}_S^*)} [f(\mathbf{x}_{\bar{S}}, \mathbf{x}_S^*)] \right| \right] \\
&= \mathbb{E} \left[ \left| \int f(\mathbf{x}_{\bar{S}}, \mathbf{x}_S^*) p_{\theta^*}(\mathbf{x}_{\bar{S}}|\mathbf{x}_S=\mathbf{x}_S^*) d\mathbf{x}_{\bar{S}} - \int f(\mathbf{x}_{\bar{S}}, \mathbf{x}_S^*) p_{data}(\mathbf{x}_{\bar{S}}|\mathbf{x}_S=\mathbf{x}_S^*) d\mathbf{x}_{\bar{S}} \right| \right] \\
&= \mathbb{E} \left[ \left| \int f(\mathbf{x}_{\bar{S}}, \mathbf{x}_S^*) \frac{p_{\theta^*}(\mathbf{x}_{\bar{S}}|\mathbf{x}_S=\mathbf{x}_S^*)}{p_{data}(\mathbf{x}_{\bar{S}}|\mathbf{x}_S=\mathbf{x}_S^*)} p_{data}(\mathbf{x}_{\bar{S}}|\mathbf{x}_S=\mathbf{x}_S^*) d\mathbf{x}_{\bar{S}} - \int f(\mathbf{x}_{\bar{S}}, \mathbf{x}_S^*) p_{data}(\mathbf{x}_{\bar{S}}|\mathbf{x}_S=\mathbf{x}_S^*) d\mathbf{x}_{\bar{S}} \right| \right] \\
&= \mathbb{E} \left[ \left| \mathbb{E}_{p_{data}(\mathbf{x}_{\bar{S}}|\mathbf{x}_S=\mathbf{x}_S^*)} \left[ \left( f(\mathbf{x}_{\bar{S}}, \mathbf{x}_S^*) \frac{p_{\theta^*}(\mathbf{x}_{\bar{S}}|\mathbf{x}_S=\mathbf{x}_S^*)}{p_{data}(\mathbf{x}_{\bar{S}}|\mathbf{x}_S=\mathbf{x}_S^*)} - f(\mathbf{x}_{\bar{S}}, \mathbf{x}_S^*) \right) \right] \right| \right] \\
&\leq \mathbb{E} \left[ \mathbb{E}_{p_{data}(\mathbf{x}_{\bar{S}}|\mathbf{x}_S=\mathbf{x}_S^*)} \left[ \left| f(\mathbf{x}_{\bar{S}}, \mathbf{x}_S^*) \frac{p_{\theta^*}(\mathbf{x}_{\bar{S}}|\mathbf{x}_S=\mathbf{x}_S^*)}{p_{data}(\mathbf{x}_{\bar{S}}|\mathbf{x}_S=\mathbf{x}_S^*)} - f(\mathbf{x}_{\bar{S}}, \mathbf{x}_S^*) \right| \right] \right] \\
&= \delta
\end{aligned} \tag{B10}$$

Thus, the statistical error is bounded with  $\varepsilon_1 + \delta$ . Finally, the estimation error bound of VAE-based approach is as follows.

$$\mathbb{E}[\|\hat{v}(S) - v(S)\|] = \frac{\sqrt{\pi}}{\sqrt{2K}} + \varepsilon_1 + \delta \tag{B11}$$

It can be seen from Eq.(eq-b-16), the error bound of VAE-based method is limited by the variational inference. Once  $D_{KL}(q_\tau(\mathbf{z}|\mathbf{x})||p_\theta(\mathbf{z}|\mathbf{x}))$  becomes large, the error of this method can not be ignored.

## REFERENCES

- [1] R. Aggarwal, V. Sounderajah, and e. a. Martin, Guy, "Diagnostic accuracy of deep learning in medical imaging: a systematic review and meta-analysis," *NPJ Digital Medicine*, vol. 4, p. 65, 2021.
- [2] Q. Qi *et al.*, "Wrinkled soft sensor with variable afferent morphology: Case of bending actuation," *IEEE Robotics and Automation Letters*, vol. 5, no. 3, pp. 4102–4109, 2020.
- [3] A. M. Ozbayoglu, M. U. Gudelek, and O. B. Sezer, "Deep learning for financial applications : a survey," *Applied Soft Computing*, vol. 93, p. 106384, 2020.
- [4] A. B. Arrieta, N. Díaz-Rodríguez, and e. a. Del Ser, Javier, "Explainable artificial intelligence (xai): concepts, taxonomies, opportunities and challenges toward responsible ai," *Applied Soft Computing*, vol. 93, p. 106384, 2020.
- [5] F. Doshi-Velez and B. Kim, "Towards a rigorous science of interpretable machine learning," *arXiv preprint arXiv:1702.08608*, 2017.
- [6] L. S. Shapley *et al.*, "A value for n-person games," *Contributions to the Theory of Games (AM-28)*, vol. 2, pp. 307–318, 1953.
- [7] E. Strumbelj and I. Kononenko, "An efficient explanation of individual classifications using game theory," *Journal of Machine Learning Research*, vol. 11, pp. 1–18, 2010.
- [8] I. E. Kumar, S. Venkatasubramanian, C. Scheidegger, and S. Friedler, "Problems with shapley-value-based explanations as feature importance measures," in *International Conference on Machine Learning*, 2020, pp. 5491–5500.
- [9] M. Sundararajan and A. Najmi, "The many shapley values for model explanation," in *International Conference on Machine Learning*, 2020, pp. 9269–9278.
- [10] D. Fryer, I. Strümke, and H. Nguyen, "Shapley values for feature selection: The good, the bad, and the axioms," *IEEE Access*, vol. 9, pp. 144 352–144 360, 2021.
- [11] S. M. Lundberg and S.-I. Lee, "A unified approach to interpreting model predictions," *Advances in Neural Information Processing Systems*, vol. 30, 2017.
- [12] I. Covert and S.-I. Lee, "Improving kernelshap: Practical shapley value estimation using linear regression," in *International Conference on Artificial Intelligence and Statistics*. PMLR, 2021, pp. 3457–3465.
- [13] E. Štrumbelj and I. Kononenko, "Explaining prediction models and individual predictions with feature contributions," *Knowledge and Information Systems*, vol. 41, pp. 647–665, 2014.
- [14] J. Chen, L. Song, M. J. Wainwright, and M. I. Jordan, "L-shapley and c-shapley: Efficient model interpretation for structured data," in *International Conference on Learning Representations*, 2019.
- [15] A. Kar, "Axiomatization of the shapley value on minimum cost spanning tree games," *Games and Economic Behavior*, vol. 38, no. 2, pp. 265–277, 2002.
- [16] O. Skibski, T. P. Michalak, T. Rahwan, and M. Wooldridge, "Algorithms for the shapley and myerson values in graph-restricted games," in *International Conference on Autonomous Agents and Multi-Agent Systems*, 2014, pp. 197–204.
- [17] L. H. B. Olsen, I. K. Glad, M. Jullum, and K. Aas, "Using shapley values and variational autoencoders to explain predictive models with dependent mixed features," *Journal of Machine Learning Research*, vol. 23, no. 1, pp. 9553–9603, 2022.
- [18] H. Chen, I. C. Covert, S. M. Lundberg, and S.-I. Lee, "Algorithms to estimate shapley value feature attributions," *Nature Machine Intelligence*, vol. 5, pp. 590—601, 2023.
- [19] Y. LeCun, S. Chopra, R. Hadsell, M. Ranzato, and F. Huang, "A tutorial on energy-based learning," *Predicting structured data*, vol. 1, no. 0, 2006.
- [20] C. Nash and C. Durkan, "Autoregressive energy machines," in *International Conference on Machine Learning*. PMLR, 2019, pp. 1735–1744.
- [21] D. H. Ackley, G. E. Hinton, and T. J. Sejnowski, "A learning algorithm for boltzmann machines," *Cognitive Science*, vol. 9, no. 1, pp. 147–169, 1985.
- [22] R. Szeliski, R. Zabih, D. Scharstein, O. Veksler, V. Kolmogorov, A. Agarwala, M. Tappen, and C. Rother, "A comparative study of energy minimization methods for markov random fields," in *European Conference on Computer Vision*. Springer, 2006, pp. 16–29.
- [23] J. Chung, C. Gulcehre, K. Cho, and Y. Bengio, "Empirical evaluation of gated recurrent neural networks on sequence modeling," in *Advances in Neural Information Processing Systems Workshop on Deep Learning*, 2014.
- [24] B. W. Silverman, *Density estimation for statistics and data analysis*. Routledge, 2018.
- [25] R. Strauss and J. B. Oliva, "Arbitrary conditional distributions with energy," *Advances in Neural Information Processing Systems*, vol. 34, pp. 752–763, 2021.
- [26] K. He, X. Zhang, S. Ren, and J. Sun, "Deep residual learning for image recognition," in *Computer Vision and Pattern Recognition*, 2016.
- [27] A. Gupta, S. Tian, Y. Zhang, J. Wu, R. Martín-Martín, and L. Fei-Fei, "Maskvit: Masked visual pre-training for video prediction," in *International Conference on Learning Representations*, 2023.
- [28] S. Zhai, Y. Cheng, W. Lu, and Z. Zhang, "Deep structured energy based models for anomaly detection," in *Proceedings of The 33rd International Conference on Machine Learning*, vol. 48. PMLR, 20–22 Jun 2016, pp. 1100–1109.
- [29] W. Grathwohl, K.-C. Wang, J.-H. Jacobsen, D. Duvenaud, M. Norouzi, and K. Swersky, "Your classifier is secretly an energy based model and you should treat it like one," in *International Conference on Learning Representations*, 2020.

- [30] W. Hoeffding, “Probability inequalities for sums of bounded random variables,” *Journal of the American Statistical Association*, vol. 58, no. 301, pp. 13–30, 1963.
- [31] B. Efron, T. Hastie, I. Johnstone, and R. Tibshirani, “Least angle regression,” *The Annals of Statistics*, vol. 32, no. 2, pp. 407 – 499, 2004.
- [32] R. Cugny, J. Aligon, M. Chevalier, G. Roman Jimenez, and O. Teste, “Autoxai: A framework to automatically select the most adapted xai solution,” in *Proceedings of the 31st ACM International Conference on Information & Knowledge Management*, no. 10, 2022, p. 315–324.
- [33] W. Yan, D. Tang, and Y. Lin, “A data-driven soft sensor modeling method based on deep learning and its application,” *IEEE Transactions on Industrial Electronics*, vol. 64, no. 5, pp. 4237–4245, 2016.
- [34] C. Villani *et al.*, *Optimal transport: old and new*. Springer, 2009, vol. 338.
- [35] X. Jiang and Z. Ge, “Augmented multidimensional convolutional neural network for industrial soft sensing,” *IEEE Transactions on Instrumentation and Measurement*, vol. 70, pp. 1–10, 2021.
- [36] G. Boole, *The mathematical analysis of logic*. Philosophical Library, 1847.
- [37] D. Garreau and U. von Luxburg, “Explaining the explainer: A first theoretical analysis of lime,” in *Proceedings of the Twenty Third International Conference on Artificial Intelligence and Statistics*, ser. Proceedings of Machine Learning Research, S. Chiappa and R. Calandra, Eds., vol. 108. PMLR, 26–28 Aug 2020, pp. 1287–1296.
- [38] H. Weyl, “Das asymptotische Verteilungsgesetz der Eigenwerte linearer partieller Differentialgleichungen (mit einer Anwendung auf die Theorie der Hohlraumstrahlung),” *Mathematische Annalen*, vol. 71, no. 4, pp. 441–479, 1912.
- [39] A. Shekhovtsov, D. Schlesinger, and B. Flach, “VAE approximation error: ELBO and exponential families,” in *International Conference on Learning Representations*, 2022.
- [40] C. Cremer, X. Li, and D. Duvenaud, “Inference suboptimality in variational autoencoders,” in *International Conference on Machine Learning*. PMLR, 2018, pp. 1078–1086.